

N O T I C E

THIS DOCUMENT HAS BEEN REPRODUCED FROM
MICROFICHE. ALTHOUGH IT IS RECOGNIZED THAT
CERTAIN PORTIONS ARE ILLEGIBLE, IT IS BEING RELEASED
IN THE INTEREST OF MAKING AVAILABLE AS MUCH
INFORMATION AS POSSIBLE

ROTATIVE BALANCE OF THE I.M.F. LILLE
AND ASSOCIATED EXPERIMENTAL TECHNIQUES

R. Verbrugge

(NASA-TM-75886) ROTATIVE BALANCE OF THE
I.M.F. LILLE AND ASSOCIATED EXPERIMENTAL
TECHNIQUES (National Aeronautics and Space
Administration) 51 p HC A04/MF A01 CSCL 14B

N81-19137

Unclas
G3/09 18843

Translation of "Balance rotative de l'I.M.F. Lille et techniques experimen-
tales associees," Association Aeronautique et Astronautique de France,
AAAF Paper NT 80-13, 16th Colloque d'Aerodynamique Appliquee, Lille,
France, Nov. 13-15, 1979, pp 1-50



1. Report No. NASA TM-75886	2. Government Accession No.	3. Recipient's Catalog No.	
4. Title and Subtitle ROTATIVE BALANCE OF THE I.M.F.LILLE AND ASSOCIATED EXPERIMENTAL TECHNIQUES		5. Report Date January 1981	
		6. Performing Organization Code	
7. Author(s) R. Verbrugge, I.M.F.Lille		8. Performing Organization Report No.	
		10. Work Unit No.	
9. Performing Organization Name and Address Leo Kanner Associates Redwood City, California 94063		11. Contract or Grant No. NASw-3199	
		13. Type of Report and Period Covered Translation	
12. Sponsoring Agency Name and Address National Aeronautics and Space Admini- stration, Washington, D.C. 20546		14. Sponsoring Agency Code	
15. Supplementary Notes Translation of "Balance rotative de l'I.M.F.Lille et techniques expérimentales associées," Association Aeronautique et Astronautique de France, "AAAF" Paper NT 80-13, 16th Colloque d'Aero- dynamique Appliquée, Lille, France, Nov. 13-15, 1979, pp 1-50 (A80-36844)			
16. Abstract The study of aerodynamic effects at high incidence associated with motions of wide amplitude incorporating continuous ro- tations requires the consideration of coupled effects which are generally nonlinear in a new formulation of equations of motion. A rotative balance designed to simulate such maneu- vers in a windtunnel was created at the I.M.F.Lille to form a test medium for analytical studies. This report provides a general description of the assembly by considering two main ranges of application: the study of flight at high incidence and upsets, the study of stalling relative to spinning. The capacities and performances of the assembly are discussed.			
17. Key Words (Selected by Author(s))		18. Distribution Statement Unclassified	
19. Security Classif. (of this report) Unclassified	20. Security Classif. (of this page) Unclassified	21. No. of Pages	22. Price

ROTATIVE BALANCE OF THE I.M.F.LILLE
AND ASSOCIATED EXPERIMENTAL TECHNIQUES

R. Verbrugge
I.M.F.Lille

ABSTRACT

The study of aerodynamic effects at high incidence associated with motions of wide amplitude incorporating continuous rotations requires the consideration of coupled effects which are generally nonlinear in a new formulation of equations of motion.

A rotative balance designed to simulate such maneuvers in a windtunnel was created at the I.M.F.Lille to form a test medium for analytical studies.

A general description of the assembly will be provided by considering two main areas of application: the study of upsets and flight characteristics at high incidence; the study of stalls relative to spins.

The capacities and performances of the assembly will be defined, notably:

- geometric characteristics and kinematics: degrees of freedom, test range,
- mechanical and structural characteristics,
- aerodynamic aspects,
- measurement-collection aspects and data processing, test procedures and analysis.

The first industrial experiences of this assembly are described in the second part of the report presented by A.M.D.-B.A.

1 - INTRODUCTION

The forecast of flight qualities and performance of modern aircraft requires the development of test means adapted to its new range of maneuvers resulting mainly from the integration of generalized automatic controls.

We must consider a very wide range of incidence/side-slip in which motions most often are of large amplitude with rotation rates which are sometimes high and in some cases continuous.

In such maneuvers the flows are complex. Accordingly, there are nonlinearities in the characteristics of stability and strong couplings between the various degrees of freedom. If the parameters of dynamic stability are practically independent from the fundamental aerodynamic magnitudes (α , β), in the range of low incidences, this is not the case at higher incidences. The variations observed are very large because they are highly related to the flow characteristics in which the definitions of local geometry may play a determining role.

These maneuvers "at high incidence" are actually the same type as those which characterize upsets, tail spins or recovery. Considering the range explored, they depend on the distribution of the zones of separation on the various airplane components and they depend on special aerodynamic interactions.

The traditional dynamic balances are not designed for the study of these effects. They actually produce derivatives in relationship with the traditional assumptions of small disturbances. In the range α , β , the mean values of p , q , r , are zero. The rotation of wide or continuous amplitude is not shown and the nature of the flow is basically different.

In order to measure the aerodynamic characteristics in this new range, the I.M.F.Lille studied and created a rotative balance

designed for the simulation of such maneuvers in a windtunnel to provide a test medium for analytical studies. This work was carried out in close collaboration with the A.B.A. and with the support of the Section Etudes Générales du Service Technique Aéronautique (General Studies Section of the Aeronautic Technical Service).

The assembly was set up over a period of 12 months and the first tests took place in September 1978.

2 - CHARACTERISTICS SPECIFIC TO THE ASSEMBLY

The I.M.F.L. rotative balance was designed to meet two types of test requirements. First, to study the "flight range at high incidences" and, second, to continue the investigation of spinning.

In the first case, relatively large models will be considered to account for Reynolds effects (range 10^6), as the rates of rotation may reach $600^\circ/\text{s}$ at the model scale and the possibility of separating the speed vector \vec{v} from vector $\vec{\Omega}$ of an angle $\hat{\lambda} = \vec{v}, \vec{\Omega}$ which may reach 20° , thus recreating motions incorporating dynamic aspects in α and β . For this type of test, the use of low speed windtunnel models was searched for, thus leading to a mean height of about 1.5 m and a mass which may reach 50 Kg.

To investigate the spinning range, the models are most often used in free spins (maximum size 0.8 m) and the degrees of freedom of the assembly must make it possible to incorporate a spinning radius and a relative heading. Due to the vertical location in the wind-tunnel, the steady spinning conditions may be directly simulated.

Wider capabilities in the area of spins are being searched for in order to investigate the effects of autorolling spins or autorolling at high incidence followed by the introduction of agitations to continuous rotations.

In any case, the assembly must permit the determination of the aerodynamic torque as a function of the parameters characterizing the motion and control surfaces. It must also make it possible to measure local stress or pressure and allow for the visualization of flows.

3 - DESCRIPTION OF THE ASSEMBLY

3.1 - General Organization

The rotary assembly is located in the test section of the large vertical windtunnel at the I.M.F.L. It is a low speed windtunnel (40 m/s maximum) with open jet section of 4 m, used until now mainly to investigate free spins and recovery on the models (see fig. 1). This unique location compared to other rotative assemblies makes it possible to minimize or eliminate, depending on the test conditions, the dynamic loads resulting from the gravitational pulse.

The mounting may be placed in the test section or disassembled (fig. 2) by using an actuating jack to elevate its position and to fasten the central pin to four beams which are virtually radial to the concrete structures of the windtunnel. By rotating a vertical pivot in the test section, the entire assembly may be placed in and out of it. It takes only a half-day to change from the test configuration of free spins to the rotative test configuration.

All operations of the windtunnel balance are controlled from a desk located above the test section. All measuring channels pass through it and are numbered. The system is connected to the data processing and collection center by cabled channel.

3.2 - Description of Operations - Degrees of Freedom - Kinematics

The diagram of the various degrees of freedom is shown in figure 3. The model is held by the 6 or 5 component dynamic balance and is mounted on the sting from the rear. (This configuration is used at an incidence reaching 60°). This sting is connected to a curved

arm. A first rotation may be obtained around the axis of the sting over 360° . This motion is motorized; the adjustment is automatic and the accuracy of the angular position is $.1^\circ$. The motion must occur without wind and without rotation. Hydraulic clamps provide the fixation rigidity which is indispensable for dynamic testing. A variant was nevertheless developed to perform measurements on spinning type models during continuous rotations in ϕ up to 20 rd/s for the entire range of incidence which may be applied to the main rotation $\vec{\Omega}$.

The curved arm is used to display angle θ (between the axis of the sting or H.F.R. and the direction parallel to vector $\vec{\Omega}$ in the plane of symmetry of the curved arm). The range considered is $0 - 45^\circ$ for the tests at high incidence, and $45^\circ - 90^\circ$ for the spinning tests. This operation is motorized, the accuracy of the angular position is more than $.1^\circ$. The adjustment may be executed without wind during shutdown. Hydraulic clamps are used for the dynamic tests.

The motions in ϕ and θ_2 do not displace the center of inertia in the test section.

The curved arm is connected to a pivot fastened to a slider.

The relative heading ψ_R may be displayed by operating around the pivot. This parameter is specific to spinning. It is adjusted manually. It may be set by a pitch of 20° in the $\pm 180^\circ$ range. It is locked manually by bolts.

The slider connected to the main axis of the assembly makes it possible to introduce the spinning radius R by a lateral displacement of the curved arm pivot. The maximum radius is 0.20 m. The operation is motorized; the adjustment is made without wind and without rotation and the value obtained is 10^{-3} m. Locking is ensured by hydraulic blocking jacks.

Rotation occurs about the main axis of the assembly. It is obtained by a continuous current motor torque, the speed of which is controlled by a tachymetric generator. The rotation may occur in both directions. Constant $\vec{\Omega}$ or laws of speed variation may be applied. The maximum speed is 11 rd/s and the display accuracy is $2 \cdot 10^{-3}$ rd/s.

The rotation is blocked at ψ_0 in order to allow for measurements of traditional polars. This plane, which contains $\vec{\Omega}$, is perpendicular to the horizontal axis allowing for rotation λ .

λ is the angle between \vec{v} and $\vec{\Omega}$. The operation is controlled by an hydraulic jack. The motion may be created with wind in order to execute the polars. The mean displacement speed is $0.75^\circ/\text{s}$.

λ may reach 30° . For the rotation tests, the maximum λ was fixed at 20° . The accuracy is continuous and the over-all display precision is more than 0.1° .

Let us recall that the maximum speed of the windtunnel is 40 m/s.

The maximum size of the model is 1.5 m.

The control surfaces of the model may be motorized, if necessary.

All controls, measuring and control channels transit through rotative electrical contacts and a high pressure hydraulic coupler located at the top of the assembly.

A table summarizing the main characteristics is shown in figure 4.

Since various parameters are displayed: δ_2 , ψ , R , λ , ψ_R a trajectory diagram of the tip sections of the model and of the C.G rotating in ψ (integral of Ω) was established for the most critical combinations. To keep these trajectories, on the average, centered on the axis of the windtunnel test section, the main hub of the assembly was offset by 0.4 m.

For the choice of motorization, the d.c. torque motor with reduction gear box without play was preferred to the hydraulic motor. The latter reconciles high torque with reduced size, but it does not have a torque of infinite angular value and it may therefore generate spurious pulses.

The remarkable characteristic of the selected torque motor and its control system is that it is capable of maintaining a speed of more than 1°/oo when the resistant torque suddenly varies by 50%. This characteristic makes it possible to operate in the presence of fluctuations of the resistant torque, particularly when the motor rotates with a high value of λ .

3.3 - Definition of the Test Range

The test range will usually be defined by the values of incidence and side-slip which are determined by defining the center of inertia of the model, the value of Ω and V fixing the propeller angle at the wing tips ($\Omega b/V$) and the projections of vector Ω in the model identification which defines p , a and r .

The precise calculation of α, β is shown in appendix I. It takes into consideration rotations λ, ψ, θ_2 and ϕ , successively, along with rotation which corresponds to a possible angular displacement (along the assembly) between the axis of the balance and the longitudinal fuselage reference.

The complex expressions obtained may be shown graphically in the form of the chart suggested in figure 5. For the case where δ is zero, in the range α 65°, β 40°, the maximum error will remain less than 1°.

It should be pointed out that when the test conditions are defined by parameters θ_2 and/or ψ only, the rotation occurs around a fixed point in the plane α, β . θ_2 determines the maximum incidence and ψ introduces side-slip β . When we display a value of λ , in a first approximation in plane α, β the motion

in ψ may be shown by a circle in the maneuvering range under consideration.

It is much easier to interpret parameters Ω and V . To represent spins, the helix angle ($\Omega b/V$) should be taken into special consideration. For studies at high incidence, each magnitude may vary separately and it is thus possible to show the effects of the Reynolds number on the reduced pulse Ω^* .

The components of vector \vec{A} in the model identification are calculated in appendix I. They taken into account the three rotations θ_2 , ϕ and δ . They are generally constant throughout a test.

Let us bear in mind that the assembly can rotate in both directions. When λ is zero, i.e. α and β are constant during the rotation, it is therefore possible to obtain a reversal of the only components p, q, r of \vec{A} . When only λ is displayed for each value of ψ in rotation Ω , the two values α β remain the same, but Ω is reversed. The over-all symmetry of the test conditions will therefore consist of comparing in plane α β the values obtained at ψ_1 given with those which are mirror-imaged around the origin: $\psi_1 + \pi$. We therefore obtain the reversal of all magnitudes α β Ω . When the test contains only θ_2 and λ , a mirror-image on β may be obtained.

In the case where θ_2 , ψ and λ are displayed simultaneously, two distinct test cases for both directions of rotation are then obtained.

Appendix 1 provides the Euler angles which are normally used in flight mechanics. They are different from ψ , θ , ϕ of the assembly as a function of the various predetermined parameters and of position ψ in the rotating model.

If we know all of these characteristic magnitudes of motion, it is possible to select a test program which may be executed within the multitude of possible combinations. A thorough inventory must be

provided for the entire useful range of the assembly, including that which is characteristic to spins.

3.4 - Mechanical and Structural Characteristics

A thorough structural study of the rotary assembly was conducted at the project stage in order to define assembly deformations under static loads and its dynamic characteristics along with those of the measuring balance. This study made it possible to define the over-all dimensioning of the assembly structures. The criteria were selected to obtain for the equipped assembly of a 50 Kg model a first structural mode at a minimum of 10 Hz.

Furthermore, in order to choose the location of the assembly, preliminary measurements were made to define the possible excitations on its foundation caused by the windtunnel operation.

3.4.1 - Excitations Caused by the Windtunnel Operation

An analysis was made of the frequency and amplitude of the vibrations recorded. The points selected for measurements were at the end of the beams supporting the top floor of the test section and at the location where the assembly should be fastened (see figure 6). They were accelerometric measurements performed horizontally and vertically on the plane perpendicular to the axis of the beam.

The analysis was made on an average of 32 spectra.

The general appearance of the amplitude spectra shows a practically nonexistent energy level in the bandwidth 0 - 100 Hz between 16 and 40 m/s, except in a few well-defined regions where Frequency F appears: number of rotations per second of motor \times , number of ventilator blades. At maximum speed, this frequency is 71 Hz. The effective acceleration is 0.6 m/s^2 and the deformation is 3μ .

A finer analysis was made in the 0 - 20 Hz bandwidth range where the fundamental of the assembly will be found. Here again, a very low average energy level may be observed. On the γ_y a spectrum line

of weak intensity is generally found. This corresponds to the motor rotation frequency (balancing residue).

A single coupling with the structure seems to be obtained at $\Omega = 230$ rpm, i.e. 28 m/s of wind on a line frequency of 4 Hz.

The weak levels of the lines observed above 9 Hz do not warrant the fears that rotary assembly has forced excitations of large amplitude.

3.4.2 - Structural Study

In order to determine the deformations of the assembly under loads, a matrix of impact coefficients was computed for a structure modelled with 5 beams. The balance under study is connected to these beams as stiffener component and is defined by its own matrix of impact coefficients. The model is connected to the beams as a pure mass component (see figure 7). The concrete beams of the windtunnel are considered to be undeformable.

The matrices define the displacement vector (δ) of this same point for torque forces (T) applied to the center of gravity of the model, according to the relationship: $(\delta) = (C) \cdot (T)$.

An example of results obtained from the numerous test cases is shown on figure 8. The reference trihedral is the model trihedral. It shows the effect of each assembly component on the deformations: beams, pin, sector, sting and balance. The curved sector and sting, which have maximum dimensioning relative to the projection of the base of the model, have considerable effect on linear deformations, δ_y and δ_z . The deformations at the center of inertia, however, are still a few millimeters for maximum loads of 1,000 Newton in Z. The balance, of course, has a predominant effect on angular deformations. For cumulative values, the angular deformations do not reach 0.2° for the maximum moments applied to the model.

Based on an analogous modelling of the assembly, the dynamic deformations and fundamental modes were also calculated. The structure was represented by a system of 7 knots and 36 degrees of freedom. The masses and inertias of the components are shown on the knots. The balance is schematized by 3 degrees of freedom and its deformation matrix.

The frequency of the fundamental mode is always close to 10 Hz for any configuration of the 50 Kg model.

This is the case of a yawing mode of the model with simultaneous displacements in Y and ψ . The second and third mode is in the 10 to 15 Hz range. In the case of a 20 Kg model, the first mode in Y would be found at about 13 Hz.

3.4.3 - Reception of the Assembly in the Test Section - Structural Characteristics

The assembly created on the basis of the description and design provided above was subjected to numerous reception tests in the windtunnel, particularly from the point of view of structural noises linked to its operation.

The deformations under static loads were checked and there is a 20% difference from the forecast for applied loads in X, Y, Z and for both positions of curved sector $\theta_{2.2} = 0$ and 45° .

The characteristics of the structural modes were brought to light by exciting the assembly and model successively for each degree of freedom by shocks and by recording the signals originating from the balance. The model mounted on the balance weighs 32 Kg.

The tests were performed for Ω and $V = 0$.

Analysis of the signals made it possible to bring to light the modes presented in figure 9. These modes are analogous to those determined by the forecast. The frequencies are found in the 10 to 21 Hz range. The modes are very moderately damped and the

pitching-pumping couplings and yawing Y are observed. This information confirms that the structural characteristics of the assembly coincide with the targets defined in this regard. From the point of view of processing rotation data, it is necessary to perform accelerometric measurements in order to identify the dynamic torque.

These investigations were completed by initial measurements of noises caused by the aerodynamic or mechanical characteristics of the windtunnel operation and of the assembly rotation in Ω .

A few typical cases are shown on figure 10. Analysis of signals from the balance by using the Fourier transform make it possible to draw the first conclusions described below.

Without wind, rotation Ω alone does not produce significant noise levels. The density increases moderately with the modulus of Ω .

Wind tests without rotation clearly bring to light that the structural modes are generally more distinguishable as α increases (case 3 and 4 figure 10).

Accordingly, the excitation originates largely from the wind-tunnel operation and more from aerodynamic characteristics than from mechanical noises transmitted to the assembly support by the ventilator motor unit. This assumption is supported by a very high correlation between the disturbances and the position in ψ of the rotating model in the test section.

Analysis of signals is performed for the mean values of a large number of successive rotations (an average of 10 rotations).

Considering the incidence-speed distribution in the section and the aerodynamic effects on the model, both of which are related to ψ , the high correlation observed between noises and the position of the model defining the instantaneous values of α , β may be partially justified.

4 - EXPERIMENTAL TECHNIQUES

4.1 - Aerodynamic Aspects

The rotary assembly is used in the SV 4 windtunnel which has been used until now for studies of free spins. For this purpose, the certification of the test section satisfies two needs. First, during free spin tests, it is possible to reduce the speed in the axis of the section to center maneuvers of the model and, second, to obtain a negative speed gradient along Z in order to automatically stabilize the model at the level of the test chamber. The section therefore diffuses at the outlet of the collector and is extended by the diffuser.

The test section was completely studied in the presence and in the absence of the rotary assembly before conducting quantitative tests in order to bring desired modifications to the aerodynamic range.

4.1.1 - Aerodynamic Noise Spectrum

We have examined in this regard only over-all aerodynamic noises of the fluid section. For this purpose static pressure measurements were performed inside the working chamber of the windtunnel. A spectral analysis of the signals is presented in figure 11; it corresponds to a single test case ($V = 35$ m/s.) for which a distinct line and high intensity appear. It is located in frequency at 9.4 Hz and undoubtedly originates from a coupling relative to the geometric dimensions of the open jet or to the aerodynamic circuit in general.

Due to the effect this excitation can have, while performing measurements on the balance we will avoid operating in this very narrow range of critical speed centered at 35 m/s.

A more localized identification of noises in the test section accompanying measurements of turbulence is considered to complete this information.

4.1.2 - Aerodynamic Interferences Assembly-Model

In order to examine possible aerodynamic interactions of the rotary assembly on measurements, two types of tests were conducted in the windtunnel at the preliminary project stage of the assembly.

In a first test conducted with S5 T₀ on model Δ 2000 at scale 1/8.6 (identical to that considered for the rotative balance), the direct aerodynamic interactions of supports closest to the model were evaluated (sting and circular sector) in order to define the positioning of the curved sector relative to the model. For this purpose, dummy supports were positioned (see figure 12) at various distances R of C.G. from the dummy without touching the dummy with the weighing model. For a distance R = 1.4 m there was no detectable interaction measured on the longitudinal coefficients and on the effectiveness of control surfaces in a range of incidence reaching 45°. Only a very small increase in stability was measured at high incidences. This was evaluated at about 5 %/oo. It could be due to the projection of the sting from the base of the model.

A second test was carried out in the SV 4 vertical windtunnel to detect the effects of induction which the rotary motion of the assembly has on the model (see figure 12).

We then observed whether the rotary support can drive the model in its design position while rotating freely.

We used a schematic model size 1/8.6 of Δ 2000 and the rotary sector is stylized by a plate representing its midship frame, which makes the tests very pessimistic.

The model is suspended by a wire and the resistant torque which must be overcome is 6.10^{-3} m.N.

The tests were conducted for $\alpha = 0$ and 90°, several reduced pulses $\Omega_{b/v}$ were performed and the test time is 60 s.

The model did not display any rotary motion. These preliminary tests have essentially confirmed that it is possible to construct the assembly according to a well defined design without the risk of special aerodynamic interferences.

Let us also point out that all structures of the rotary assembly obstructed the test section by a relative maximum of 6%. This is not detrimental when the test configuration is taken into consideration.

4.1.3 - Explorations of the Aerodynamic Range of the Test Section

Aerodynamic Corrections

Extensive explorations of the aerodynamic range of the test section were carried out by direct methods: anemoclinometry, flow visualizations for the purpose of adjusting the test section to obtain satisfactory aerodynamic characteristics in the presence of the assembly.

We have studied the heterogeneity of kinetic pressure q_0 , the "drift" of section $\Delta\alpha$, the static pressure gradient (capable of influencing the flows) in the absence of the assembly and in the presence of the latter for various positions ψ , θ_2 , λ and in the entire range scanned by the model.

Preliminary Explorations

Figure 13 shows for the test section configuration without assembly the kinetic pressure distributions obtained for two wind velocities 20 and 40 m/s measured along 4 diameters and 3 heights. The horizontal distribution is good, only a weak negative vertical gradient of 2 to 3% over 2 m. is measured which is justifiable for tests of free spins. It was not necessary to modify this basic configuration: test section without assembly.

Figure 14 shows the results obtained for kinetic pressure distributions in the presence of the assembly and for a mean position of the

model ($\psi = 0$, $\theta_2 = 45^\circ$, $\psi = 0$, $\lambda = 0$) with the test section in the original configuration.

This time the vertical gradient is very pronounced in the axis of the test section where it exceeds 15% over 2 m. The distribution which is horizontal to the base still remains correct. To attenuate the effects of by-passing caused by the localized obstruction due to the presence of the assembly, the test section was contracted at the level of the collector outlet plane by operating the flaps located in this area which are used to guide the section along the vertical line.

The results obtained by this contraction are shown on figure 15. The axial velocity gradient is corrected by producing a contraction ratio for the collector outlet section of 0.985. Accordingly, between the forward tip of the model and the trailing edge, i.e. about 1.5 m, the kinetic pressure ratio is less than 3%. The horizontal distribution is still correct, except in regions very close to the assembly by-pass where excessive speeds appear. They are not, however, in the maneuvering range of the model.

Detailed Explorations

They are warranted by the fact that the assembly may assume highly diverse positions: motions ψ , θ_2 or λ which displace the curved sector in the test section. Moreover, for ψ and λ the C.G. of the model shifts within the section. Selection of a kinetics "reference" was therefore questioned along with the definition of the section drift.

More extensive measurements in the maneuvering range of the model were performed and the main results are shown in figure 16. They account for more than 300 measurements for various configurations. The kinetic pressure reference taken on the C.G. model and related to an upstream kinetics does not vary for any configuration (standard deviation .007).

Furthermore, a positive static pressure gradient equivalent to .3 m bar per meter at 40 m/s is observed. Even though it is low, the gradient may possibly induce separation or a premature appearance of eddies. No simple remedy seems possible in this regard.

Clinometric measurements were performed for various configurations in the maneuvering range of the model (figure 16). Local variations $\Delta \alpha$ called a "section drift" of 1 to 2° maximum in the range explored were visible. We were not able to find a valid formulation of correction laws to account for the various positioning parameters of the assembly. The quality of such measurements is uncertain. Visualizations by using wool threads along the entire section accompanied these measurements.

Based on this information, it did not seem useful to define the spatial ventilation of the section drift. It seemed preferable to refer to over-all characteristics (polar) obtained on the model for various scanning configurations and to check the consistency of aerodynamic corrections relative to the clinometry.

Over-all Method of Aerodynamic Corrections

The over-all procedure makes it possible to separate the effects of each parameter $\theta_2, \lambda, \psi, \dots$ and to provide an accurate formulation of the correction laws which must be considered by comparing the measuring results.

Polars were made for the different test cases shown on figure 17.

The kinetic pressure at the C.G. is constant ($\sigma = .007$). The different aerodynamic characteristics obtained were compared ($C_z(\alpha), C_m(C_z)$ etc ...). On the whole, the maximum deviations observed correspond to correction terms representing lateral deviations in the section which are within a 1.5° angle for extreme cases of range $\varphi, \lambda, \theta_2, \psi$.

Figure 18 corresponds to case 6, plate 17 illustrates one of the characteristics of these tests. It is concerned with the influence of ψ and makes it possible to determine one of the components of the section drift.

The test is conducted with $\varphi = 0$, $\lambda = 0$. θ_2 is $9^\circ.26$ weak and therefore corresponds to the incidence which is therefore constant in the rotary motion. From unfiltered recordings we have calculated C_z and C_y shown as a function of ψ on the graph of figure 18. C_z and C_y are not constant. We find a symmetry around axis $\psi = \frac{\pi}{4}$ for C_z and $\psi = \frac{\pi}{4} + \frac{\pi}{2}$ for C_y . This clearly indicates the direction and modulus of the section side-drift which we were looking for.

Based on all tests conducted, a complete formulation of correction terms used in measurements with or without rotation were developed (terms $\Delta\alpha$ and $\Delta\beta$) which define values α , β corrected of the effects of all parameters shown. The exact formulation is shown in appendix 2. Special consideration was given to a sloping angle of trajectory $\hat{\gamma} = \hat{V} \cdot \hat{Z}$ associated with the corrective terms developed from values ψ , θ_2 , λ , φ .

If we apply these corrections to all polars established, we obtain unique characteristics. The spread is not greater than $.15^\circ$ on α , β and is therefore not distinguishable from the over-all measurement duplicability. Let us bear in mind that the modulus of these corrections is a maximum of 1° in $\Delta\alpha$ or $\Delta\beta$. No other aerodynamic correction is applied to the measurements. Let us also point out that in the case of $\Delta 2000$ at $1/8.6$ the Reynolds number of the tests is $2.5 \cdot 10^6$. In the report following the next paragraph a few aerodynamic characteristics and conclusions of the airplane manufacturer will be presented in this regard.

4.2 - Present Characteristics of Measurement and Data Processing

The strategy used today for measuring and processing data is based on the first industrial works carried out on the rotative

balance for the Mirage 2000. It includes the various aspects of this program and the basic characteristics of the balance, the model and the test range under consideration.

4.2.1 - Development of the Test

Stationary identifications are made prior to any testing of rotary motion in order to check the entire device, including aerodynamic corrections. They are carried out by scanning in continuous λ (0.7°/s) or by θ_2 with and without ψ for two headings ψ .

The parameters corresponding to the rotation test are displayed without wind and without rotation (see test range paragraph 3.3). A rotation test sequence therefore consists of collecting all measurements taken with wind and those taken without wind which are bound by zeros (similar procedure for polars). This procedure makes it possible to check the measurement taken with wind by comparing the zeros and determining the torque of inertia forces.

Measurements are taken for several successive rotations in order to obtain mean values in an "interval" in ψ of the determined pitch. This is indispensable in the case of tests with $\lambda \neq 0$ as α , β varies in the rotary motion.

4.2.2 - Type of Data - Measuring and Collection Process

The flow chart of the measuring process is shown in figure 19. These data are obtained from the transducers on board: 5 or 6 component balance, positions ψ , θ_2 , control surfaces and possibly anemoclinometric probes, model accelerometry or local pressures, etc. or from ground transducers: ψ_0 , Ω , q_{ref} ... All signals from transducers on board are transmitted through a rotary switch in the control room where ground information is transmitted and where conditioners of balance bridges are found. A low pass analog filter is operated at this level on different channels with a frequency close to half the digitization frequency when using 150 Hz, 12 dB filters. The signals are then digitized by PCM coder.

A visualization of the analog and digital signals is available for each parameter.

The data is then transmitted to the collection and processing center by cable.

A PPM control device may be used during the tests to loop actuators arranged on the model.

The main characteristics of the measuring device are: there are up to 30 channels with sub-cycling capability. The word length is 12 bits; the maximum pass band is 200 Hz per channel and the over-all systems accuracy is 10^{-3} .

4.2.3 - Current Data Processing

The summary of the present processing procedure is shown on figure 20.

After checking the basic signals by controlling synchronous losses and possible saturations, an optional reverse-direct low-pass filter may be used to eliminate possible high frequency noises.

Mean values are then calculated inside the intervals currently defined by $\Delta\alpha = 1^\circ$ for tests without rotation (polars made by scanning) and by $\Delta\psi \simeq 3^\circ$ for rotations. The size of the latter makes it possible to match the definition of measurements (α , β vary little in this range) with computer memory capacities for the calculations.

After checking the dynamic torque and calculating the mean value of the "zeros", we find the difference between the tests with wind and the mean value of the "zeros" without wind.

According to the tests, signals with relatively intense noise levels appear at this stage. The frequential analysis of these signals is carried out by using the Fourier transform

(F.F.T.) in conversational mode with visualization of spectra and choice of filtering options, the principles of which are: low-pass filtering, band-rejection filter or line-rejection filter. A low-pass filter applied to all signals of the balance was selected for the first tests in order to ensure a "homogeneous" processing of all data (see 4.2.4).

After passing through the balance matrix and taking into account the calibrations of all transducers, the magnitudes prepared are recovered: all coefficients, over-all aerodynamic characteristics related the characteristic values α , β , $\dot{\alpha}$, $\dot{\beta}$, p , q , r , ψ , θ , φ .

4.2.4 - Specific Characteristics of the Measuring Procedure and Data Processing

One of the main concerns of measuring and processing data in their present form lies in the frequential aspect of the problem of eliminating the various types of noises from the measurement.

A few remarks in this regard are shown on figure 21.

The rotational test range covers $0 < |\Omega| \leq 600^\circ/\text{s}$.

The procedure of using mean values in "intervals" (of about 3°) does not behave like a filter at maximum frequencies, but like a second sampling system added to that of quantifying signals made by the PCM system. Furthermore, the equivalence between the frequential analysis of the continuous signal and that of the same quantified signal must be established in order to check the F.F.T. filter. Such a precaution would imply an "optimum interval" size proportional to the rotation speed Ω , whereas the opposite logic would be used with regard to the variation of parameters α , β . The computer memory limits must also be considered.

Mean values in standard "intervals" therefore create a "lamination" for low Ω with possible frequency changes and the structural modes in bandwidth 10 - 20 Hz can appear only between 60 to $120^\circ/\text{s}$.

The maximum frequency identifiable by the F.F.T in this bandwidth does not cover all structural modes. They therefore cannot be correctly eliminated.

The sampling frequencies were adapted to the speed ranges in order to obtain a realistic number of points per interval and per channel for a given number of rotations which does not lead to an excessive collection volume.

The F.F.T. low-pass 10 Hz type filtering procedure for all of the first tests performed was adopted on the basis of specific conditions (model, balance, structure, ...).

To illustrate the importance of choosing the appropriate processing procedure, figure 22 shows part of the plot variation of a coefficient as a function of ψ (circular diagram). A sudden amplitude variation during the rotation is measured for two given values α, β . A careful measurement of such "transitions", which are the aerodynamic effects to be identified, requires a special adaptation of the data preparation procedures. Possible solutions are:

- a specific adaptation of the model-balance assembly to this type of test,
- selection of an interval size which is adapted to Ω and to the definition of dynamic terms $\dot{\alpha}, \dot{\beta}$,
- the use of direct accelerometric measurements on the model to define the dynamic torque,
- the use of filtering methods on the model whenever the model exists.

5 - CONCLUSION

About one year after it was decided to construct the rotative balance, reception tests in the section were executed. They were followed by the first industrial experiences, the results of which will be presented by Mr. COUEDOR of the A.M.D.-BA.

This new device can be adapted and developed. It is presently being designed for the investigation of auto-rolling at high incidences with or without rotation. Later on, agitations may be added to the continuous rotations.

The present design of this assembly makes it possible to compile a new data base which is needed in order to investigate the present maneuvering range of airplanes, including stationary spins. An analysis will provide a better understanding of phenomena which are now obtained from pure observations.

Next to the over-all measurements, the basic question is the following: what would be the models for such maneuvers?



CALCULATION OF α AND β

Earth Marking $\{x_0, y_0, z_0\}$

We have: Model Marking : $\{x, y, z\}$

$$\frac{\vec{V}}{x, y, z} \mid \frac{\vec{V}}{x_0, y_0, z_0} \mid \frac{\vec{V}}{V}$$

$$\begin{bmatrix} \mu \\ \nu \\ w \end{bmatrix} = \begin{bmatrix} M \\ N \\ V \end{bmatrix} \begin{bmatrix} 0 \\ 0 \\ V \end{bmatrix} \quad [M] = \begin{bmatrix} m_{11} & m_{12} & m_{13} \\ m_{21} & m_{22} & m_{23} \\ m_{31} & m_{32} & m_{33} \end{bmatrix}$$

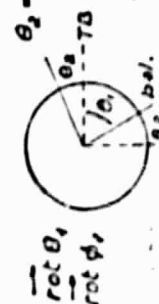
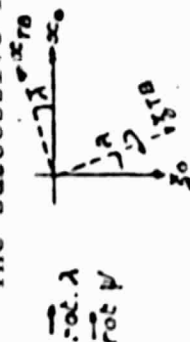
$$\begin{aligned} \mu &= m_{13} \cdot V \\ \nu &= m_{23} \cdot V \\ w &= m_{33} \cdot V \end{aligned}$$

$$\beta = \arcsin \frac{\nu}{V} = \arcsin m_{23} = \beta$$

$$\alpha = \arcsin \frac{w}{\mu} = \arcsin \frac{m_{33}}{m_{13}} = \alpha$$

Appendix 1.1

The successive rotations to be considered are: $\lambda, \mu, \theta_2, \phi, \delta$



$$\begin{bmatrix} x_0 \\ y_0 \\ z_0 \end{bmatrix}$$

$$\begin{bmatrix} x \\ y \\ z \end{bmatrix} = \begin{bmatrix} \cos \theta_2 \cos \lambda + \cos \theta_2 \sin \lambda \\ \sin \theta_2 \cos \lambda + \sin \theta_2 \sin \lambda \\ \cos \theta_2 \cos \lambda + \cos \theta_2 \sin \lambda \end{bmatrix} \begin{bmatrix} x_0 \\ y_0 \\ z_0 \end{bmatrix}$$

$$\begin{aligned} m_{13} &= \cos \delta (\cos \theta_2 \cos \lambda + \sin \theta_2 \cos \lambda \sin \lambda) + \sin \delta (\sin \theta_2 \cos \lambda + \cos \theta_2 \cos \lambda \sin \lambda) \\ m_{23} &= \sin \phi \cos \theta_2 \cos \lambda + \cos \phi \sin \theta_2 \cos \lambda + \sin \phi \sin \theta_2 \cos \lambda \\ m_{33} &= \sin \delta (\cos \theta_2 \cos \lambda + \sin \theta_2 \cos \lambda \sin \lambda) + \cos \delta (\sin \theta_2 \cos \lambda + \cos \theta_2 \cos \lambda \sin \lambda) \end{aligned}$$

$$\alpha = \arcsin \frac{A \sin \delta}{A \cos \delta + B \sin \delta}$$

$$\beta = \arcsin [\sin \lambda (\sin \mu \cos \phi + \cos \mu \sin \phi \cos \theta_2) + \cos \lambda \sin \phi \sin \theta_2]$$

COMPUTATION OF $p \ q \ r$

3 rotations are considered : θ_2 sector ϕ Balance δ off-set in this order

Appendix 1.2

$$\begin{Bmatrix} p \\ q \\ r \end{Bmatrix} = \begin{bmatrix} \cos \delta & 0 & -\sin \delta \\ 0 & 1 & 0 \\ \sin \delta & 0 & \cos \delta \end{bmatrix} \begin{bmatrix} 1 & 0 & 0 \\ 0 & \cos \phi & \sin \phi \\ 0 & -\sin \phi & \cos \phi \end{bmatrix} \begin{bmatrix} \sin \theta_2 & 0 & \cos \theta_2 \\ 0 & 1 & 0 \\ -\cos \theta_2 & 0 & \sin \theta_2 \end{bmatrix} \begin{Bmatrix} 0 \\ 0 \\ \Omega \end{Bmatrix}$$

Model Marking Balance Marking

$$\begin{Bmatrix} p \\ q \\ r \end{Bmatrix} = \begin{bmatrix} \cos \delta \sin \theta_2 + \sin \delta \cos \phi \cos \theta_2 \\ -\sin \phi \cos \theta_2 \\ \sin \delta \sin \theta_2 - \cos \delta \cos \phi \cos \theta_2 \end{bmatrix} \begin{bmatrix} \sin \delta \sin \phi \\ \cos \phi \\ -\cos \delta \sin \phi \end{bmatrix} \begin{bmatrix} \cos \delta \cos \theta_2 - \sin \delta \cos \phi \sin \theta_2 \\ \sin \phi \sin \theta_2 \\ \sin \delta \cos \theta_2 + \cos \delta \cos \phi \sin \theta_2 \end{bmatrix} \begin{Bmatrix} 0 \\ 0 \\ \Omega \end{Bmatrix}$$

$$\begin{aligned} p &= (\cos \delta \cos \theta_2 - \sin \delta \cos \phi \sin \theta_2) \Omega \\ q &= \sin \phi \sin \theta_2 \Omega \\ r &= (\sin \delta \cos \theta_2 + \cos \delta \cos \phi \sin \theta_2) \Omega \end{aligned}$$

CALCULATION OF THE EULER ANGLES

The Euler angles are ψ_0 , θ_0 , ϕ_0 . They are different from ψ , θ , ϕ used until now for the balance

We have:

$$\begin{Bmatrix} x \\ y \\ z \end{Bmatrix} = \begin{bmatrix} \cos \theta_0 \cos \psi_0 \\ \sin \phi_0 \sin \theta_0 \cos \psi_0 - \cos \phi_0 \sin \psi_0 \\ \cos \phi_0 \sin \theta_0 \cos \psi_0 + \sin \phi_0 \sin \psi_0 \end{bmatrix} \begin{bmatrix} \cos \theta_0 \sin \psi_0 \\ \sin \phi_0 \sin \theta_0 \sin \psi_0 + \cos \phi_0 \cos \psi_0 \\ \cos \phi_0 \sin \theta_0 \sin \psi_0 - \sin \phi_0 \cos \psi_0 \end{bmatrix} \begin{Bmatrix} x_0 \\ y_0 \\ z_0 \end{Bmatrix}$$

We also have predetermined:

$$\begin{Bmatrix} x \\ y \\ z \end{Bmatrix} = \begin{bmatrix} m_{11} & m_{12} & m_{13} \\ m_{21} & m_{22} & m_{23} \\ m_{31} & m_{32} & m_{33} \end{bmatrix} \begin{Bmatrix} x_0 \\ y_0 \\ z_0 \end{Bmatrix}$$

We therefore obtain:

$$\theta_0 = -\arcsin (A \cos \delta + B \sin \delta)$$

(See definition of A and B)

$$\phi_0 = \arcsin \frac{m_{23}}{m_{33}}$$

$$\phi_0 = \arcsin \frac{\sin \phi \cos \theta_2 \cos \psi \sin \lambda + \cos \phi \sin \psi \sin \lambda + \sin \phi \sin \theta_2 \cos \lambda}{A \sin \delta - B \cos \delta}$$

$$\psi_0 = \arcsin \frac{m_{12}}{m_{11}}$$

$$\psi_0 = \arcsin \frac{\cos \delta \sin \theta_2 \sin \psi + \sin \delta (\cos \phi \cos \theta_2 \sin \psi + \sin \phi \cos \psi)}{\cos \delta (\sin \theta_2 \cos \psi \cos \lambda + \cos \theta_2 \sin \lambda) + \sin \delta (\cos \phi \cos \theta_2 \cos \psi \cos \lambda - \sin \phi \sin \theta_2 \sin \lambda - \cos \phi \sin \theta_2 \sin \lambda)}$$

Appendix 2.1 - ROTATIVE BALANCE

Calculation of corrected α and β

The speed of the model relative to the wind is:

$$\begin{array}{c|c} \vec{V} & u \\ \hline x y z & w \end{array} \quad \begin{array}{c|c} \vec{V} & u_0 \\ \hline x_0 y_0 z_0 & w_0 \end{array} \quad \begin{array}{l} (x, y, z) = \text{Model Marking} \\ (x_0, y_0, z_0) = \text{Earth Marking} \end{array}$$

The calculations take into account the spatial ventilation of the section drift. Even though the windtunnel is vertical, it is found that components u_0 and v_0 are not zero.

The actual incidence is equal to the displayed incidence minus the slope of the trajectory:

$$\alpha = \alpha_0 - \gamma$$

This is not the case for side-slip.



The corrections correspond to the horizontal components of the slope of the actual trajectory; they are established as follows:
-correction $\Delta\alpha_1$ projected on axes x_0 and y_0 gives the following correction in these 2 axes:

$$R = -.007405 - .00707 \Theta_2^{rd}.$$

-correction $\Delta\alpha_2$ projected on axis x_0 only, gives the correction:

$$S = .041 \lambda^{rd} + \underbrace{.075 (\lambda^{rd} - .2967)}_{\text{if } \lambda > .2967^{rd}}$$

If we assume that $[M]$ is the matrix of transition from the ground marking to the model marking, with:

Appendix 2.2

$$[M] = \begin{bmatrix} m_{11} & m_{12} & m_{13} \\ m_{21} & m_{22} & m_{23} \\ m_{31} & m_{32} & m_{33} \end{bmatrix}$$

We have:

$$\begin{bmatrix} u \\ v \\ w \end{bmatrix} = [M] \begin{bmatrix} -(R+S)V \\ -RV \\ V \end{bmatrix}$$

$$\alpha = \arctg \frac{w}{u} = \arctg \frac{-m_{31}(R+S) - m_{32}R + m_{33}}{-m_{11}(R+S) - m_{12}R + m_{13}}$$

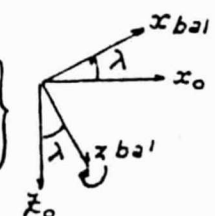
$$\beta = \arcsin \frac{v}{V} = \arcsin (-m_{21}(R+S) - m_{22}R + m_{23})$$

Calculation of matrix [M]:

We begin with the ground marking until we reach the model. The successive rotations to be considered are:

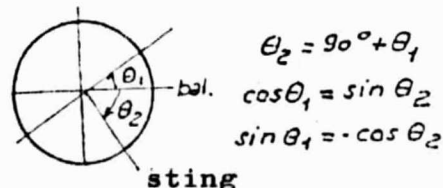
$(\vec{\Omega}, \vec{V})$	ψ	θ_2	ϕ	δ
	Heading	Sector	Sting	Balance Offset

$\left. \begin{array}{l} \vec{\text{rot}} \lambda \\ \vec{\text{rot}} \psi \end{array} \right\}$

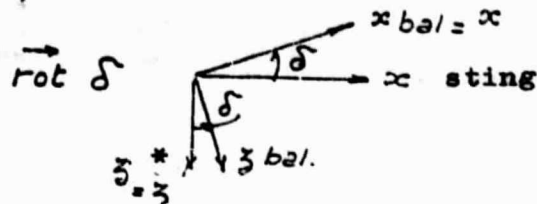


$$\begin{bmatrix} x_{bal} \\ y_{bal} \\ z_{bal} \end{bmatrix} = \begin{bmatrix} \cos \psi & \sin \psi & 0 \\ -\sin \psi & \cos \psi & 0 \\ 0 & 0 & 1 \end{bmatrix} \begin{bmatrix} \cos \lambda & 0 & -\sin \lambda \\ 0 & 1 & 0 \\ \sin \lambda & 0 & \cos \lambda \end{bmatrix} \begin{bmatrix} x_0 \\ y_0 \\ z_0 \end{bmatrix}$$

The angle between $x_{bal.}$ and x_{sting} is not θ_2 , but rather its auxiliary θ_1 and therefore:



$$\left. \begin{matrix} \vec{rot} \theta_2 \\ \vec{rot} \phi \end{matrix} \right\} \begin{bmatrix} x * \\ y * \\ z * \end{bmatrix} = \begin{bmatrix} 1 & 0 & 0 \\ 0 & \cos \phi & \sin \phi \\ 0 & -\sin \phi & \cos \phi \end{bmatrix} \begin{bmatrix} \sin \theta_2 & 0 & \cos \theta_2 \\ 0 & 1 & 0 \\ -\cos \theta_2 & 0 & \sin \theta_2 \end{bmatrix} \begin{bmatrix} \cos \psi \cos \lambda & \sin \psi & -\cos \psi \sin \lambda \\ -\sin \psi \cos \lambda & \cos \psi & \sin \psi \sin \lambda \\ \sin \lambda & 0 & \cos \lambda \end{bmatrix} \begin{bmatrix} x_0 \\ y_0 \\ z_0 \end{bmatrix}$$



$$\begin{bmatrix} x \\ y \\ z \end{bmatrix} = \begin{bmatrix} \cos \delta & 0 & -\sin \delta \\ 0 & 1 & 0 \\ \sin \delta & 0 & \cos \delta \end{bmatrix} \begin{bmatrix} \sin \theta_2 & 0 & \cos \theta_2 \\ -\sin \phi \cos \theta_2 & \cos \phi & \sin \phi \sin \theta_2 \\ -\cos \phi \cos \theta_2 & -\sin \phi & \cos \phi \sin \theta_2 \end{bmatrix} \begin{bmatrix} x_0 \\ y_0 \\ z_0 \end{bmatrix}$$

$$\begin{bmatrix} x \\ y \\ z \end{bmatrix} = \begin{bmatrix} \cos \delta & 0 & -\sin \delta \\ 0 & 1 & 0 \\ \sin \delta & 0 & \cos \delta \end{bmatrix} \begin{bmatrix} \sin \theta_2 \cos \psi \cos \lambda + \cos \theta_2 \sin \lambda & \dots & \dots \\ -\sin \phi \cos \theta_2 \cos \psi \cos \lambda - \cos \phi \sin \psi \cos \lambda + \sin \phi \sin \theta_2 \sin \lambda & \dots & \dots \\ -\cos \phi \cos \theta_2 \cos \psi \cos \lambda + \sin \phi \sin \psi \cos \lambda + \cos \phi \sin \theta_2 \sin \lambda & \dots & \dots \end{bmatrix} \begin{bmatrix} x_0 \\ y_0 \\ z_0 \end{bmatrix}$$

$$\begin{bmatrix} x \\ y \\ z \end{bmatrix} = \begin{bmatrix} \cos \delta & 0 & -\sin \delta \\ 0 & 1 & 0 \\ \sin \delta & 0 & \cos \delta \end{bmatrix} \begin{bmatrix} A & B & C \\ D & E & F \\ G & H & I \end{bmatrix} \begin{bmatrix} x_0 \\ y_0 \\ z_0 \end{bmatrix}$$

$$\begin{bmatrix} x \\ y \\ z \end{bmatrix} = \begin{bmatrix} \cos \delta & 0 & -\sin \delta \\ 0 & 1 & 0 \\ \sin \delta & 0 & \cos \delta \end{bmatrix} \begin{bmatrix} A & B & C \\ D & E & F \\ G & H & I \end{bmatrix} \begin{bmatrix} x_0 \\ y_0 \\ z_0 \end{bmatrix}$$

Which gives us: m_{ij} , $i = 1 \dots 3$, $j = 1 \dots 3$

Key: * = sting.

Appendix 2.3

We finally obtain:

$$\begin{aligned}
 \underline{\alpha = \arctan} & \left\{ \begin{aligned} & - [\sin \delta (\sin \theta_2 \cos \psi \cos \lambda + \cos \theta_2 \sin \lambda) + \dots] \\ & - [\sin \delta (\sin \theta_2 \sin \psi) + \cos \delta (-\cos \phi \cos \theta_2 \sin \psi - \sin \phi \cos \psi)] R \\ & + [\sin \delta (-\sin \theta_2 \cos \psi \sin \lambda + \cos \theta_2 \cos \lambda) + \dots] \\ & \dots \cos \delta (-\cos \phi \cos \theta_2 \cos \psi \cos \lambda + \sin \phi \sin \psi \cos \lambda + \cos \phi \sin \theta_2 \sin \lambda)] (R+S) \\ & \dots \dots \dots \\ & \dots \cos \delta (\cos \phi \cos \theta_2 \cos \psi \sin \lambda - \sin \phi \sin \psi \sin \lambda + \cos \phi \sin \theta_2 \cos \lambda)] \end{aligned} \right. \\
 & \hline \\
 & \left\{ \begin{aligned} & - [\cos \delta (A) - \sin \delta (G)] (R+S) \\ & - [\cos \delta (B) - \sin \delta (H)] R \\ & + [\cos \delta (C) - \sin \delta (I)] \end{aligned} \right. \\
 \\
 \underline{\beta = \arcsin} & \left\{ \begin{aligned} & - [-\sin \phi \cos \theta_2 \cos \psi \cos \lambda - \cos \phi \sin \psi \cos \lambda + \sin \phi \sin \theta_2 \sin \lambda] (R+S) \\ & - [-\sin \phi \cos \theta_2 \sin \psi + \cos \phi \cos \psi] R \\ & + [-\sin \phi \cos \theta_2 \cos \psi + \cos \phi \sin \psi] \sin \lambda + \sin \phi \sin \theta_2 \cos \lambda \end{aligned} \right.
 \end{aligned}$$

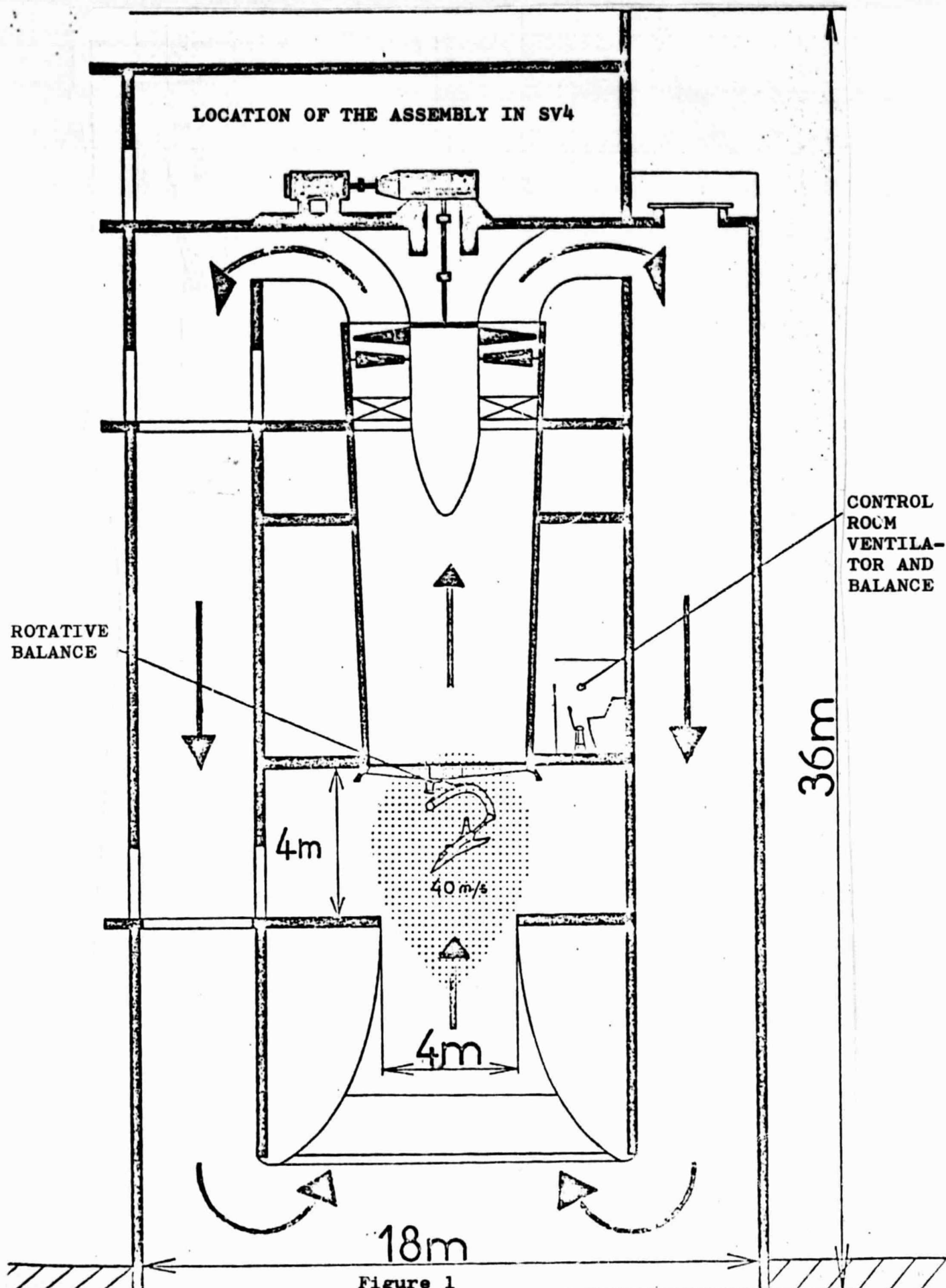
Important Remark: In R , θ_2 is that of the model when $\phi = 0$
 In m_{ij} , θ_2 is that of the angular coder.

$$\underline{\theta_2 \text{ coder} = \theta_2 \text{ mag} \cdot -\delta}$$

(definition corresponding
 to case $\phi = 0$, but
 extended to any ϕ)

ORIGINAL PAGE IS
 OF POOR QUALITY

FIGURES



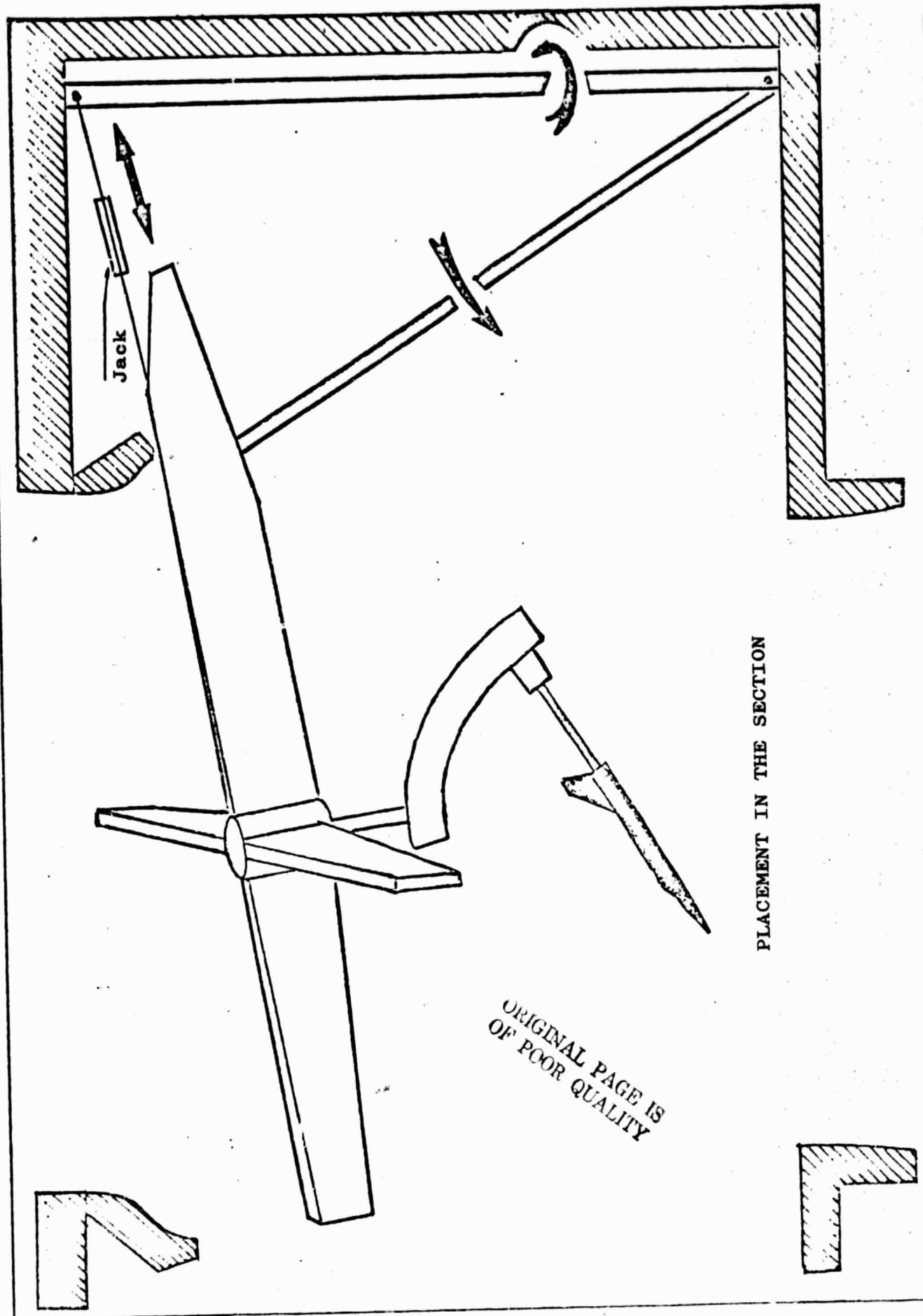


Figure 2

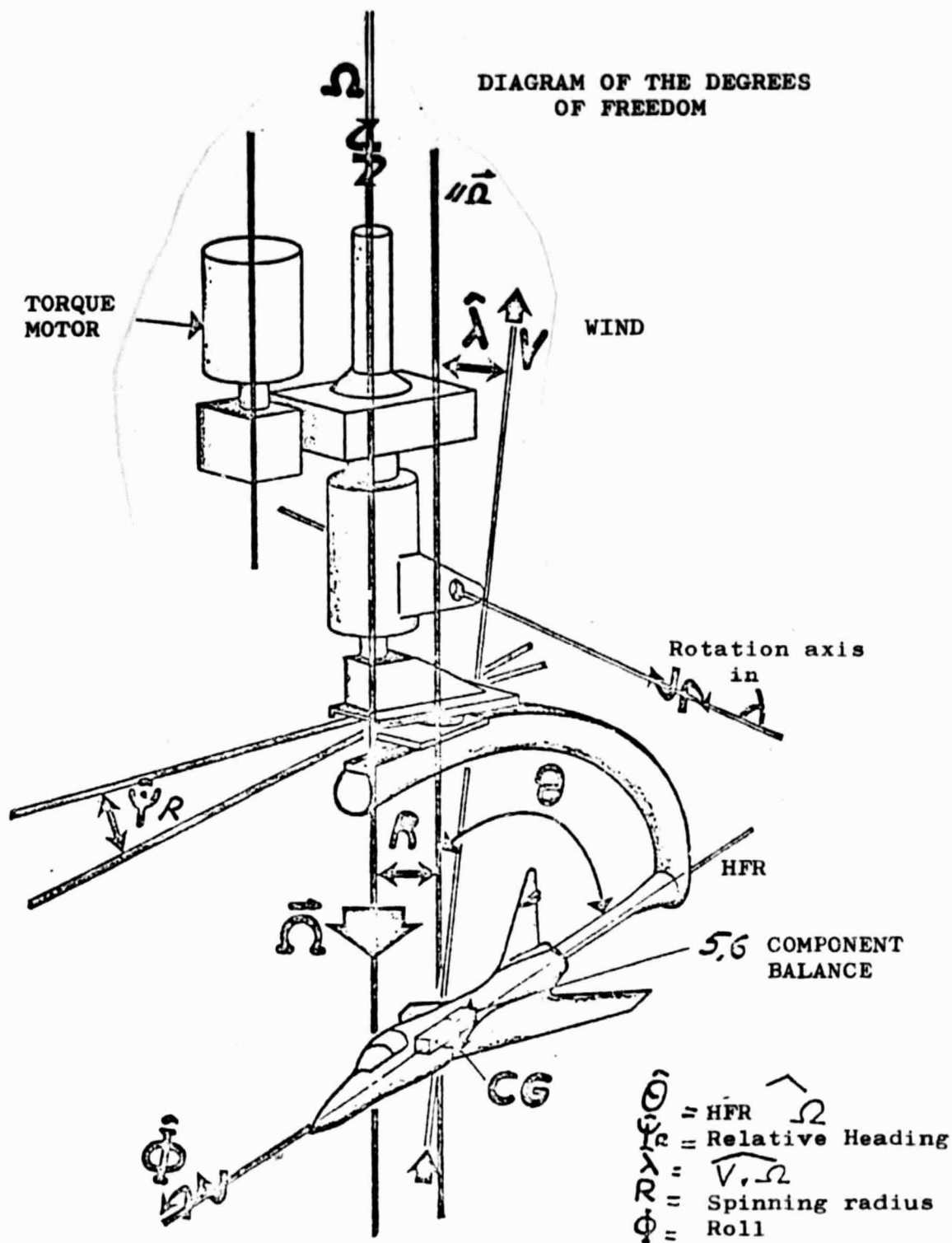


Figure 3

MAIN CHARACTERISTICS OF THE BALANCE

PARAMETERS	ADJUSTMENT			DEFINITION	DATA COLLECTED
	RANGE	AUTO	WITH WIND		
V	40 m/s	X	X	Continuous	-All test parameters: direct digital measurement.
Ω	$\pm 11 \text{ rad/s}$	X	X	" .1°/s	-5 or 6 component balance.
λ	$\leq 30^\circ$	X	X	" .1°	9 channels for accelerometers
θ	0°-45° 45°-90°	X		" .1°	-Measurements of pressure - local forces (on tail units - control surfaces).
Φ	$\pm 180^\circ$	X	X	" .1°	
R	.2 m	X		Contin. 10^{-3} m	-Visualization of flows.
ψ_R	$\pm 180^\circ$			" .1°	-All data in digits: 30 channels Length of words 12 bits 200 Hz per channel
MODEL MASS	< 50 kg			4.10 ⁻⁴	
DIMENSION	1.5 m				
POSITION OF CONTROL SURFACES	$\delta_{\theta, m, n}$	X	X	" .1°	

ORIGINAL PAGE IS
OF POOR QUALITY

Figure 4

DETERMINATION OF THE TEST RANGE

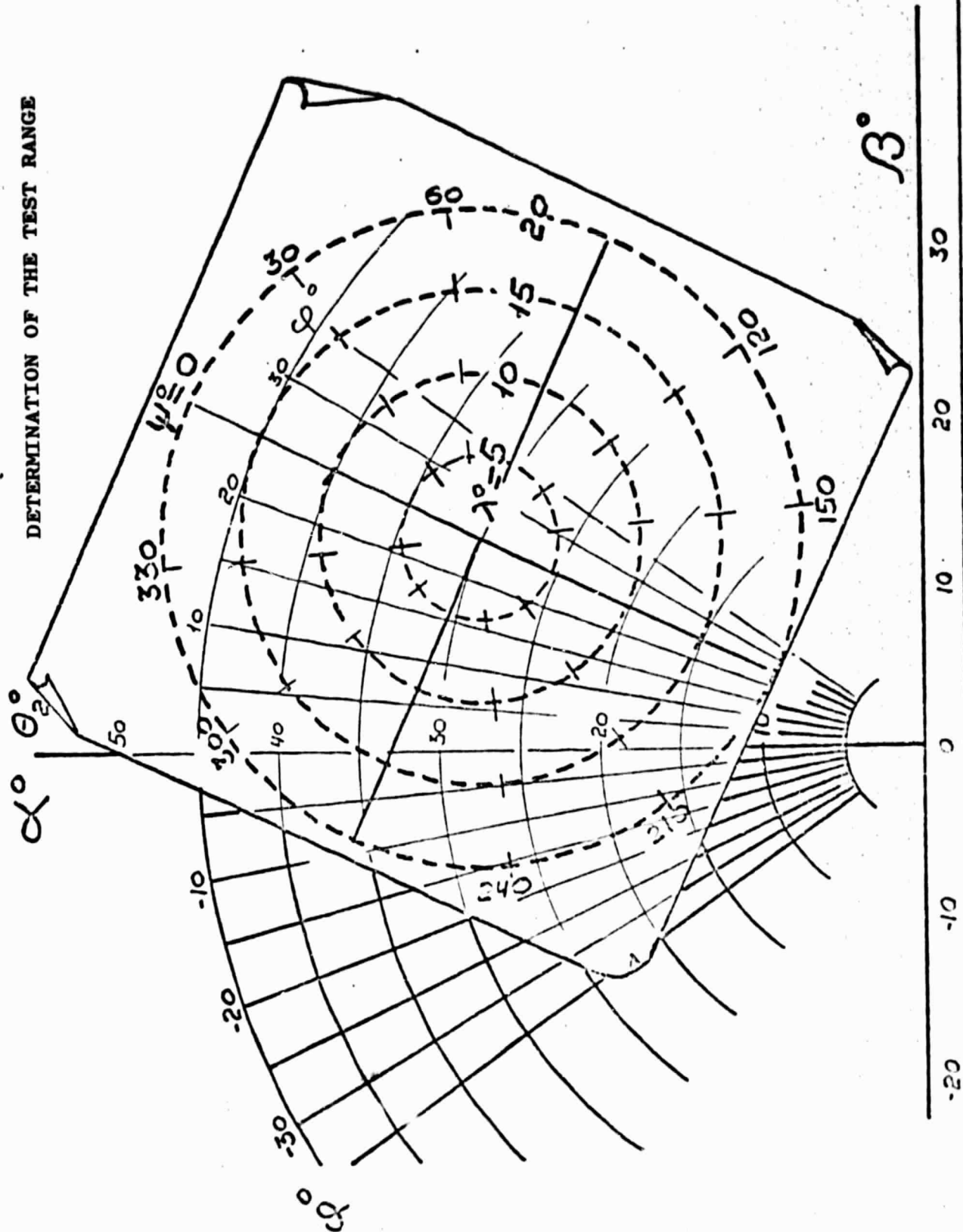


Figure 5

LOCATION OF THE ASSEMBLY
Excitations caused by the motor -
ventilator unit.

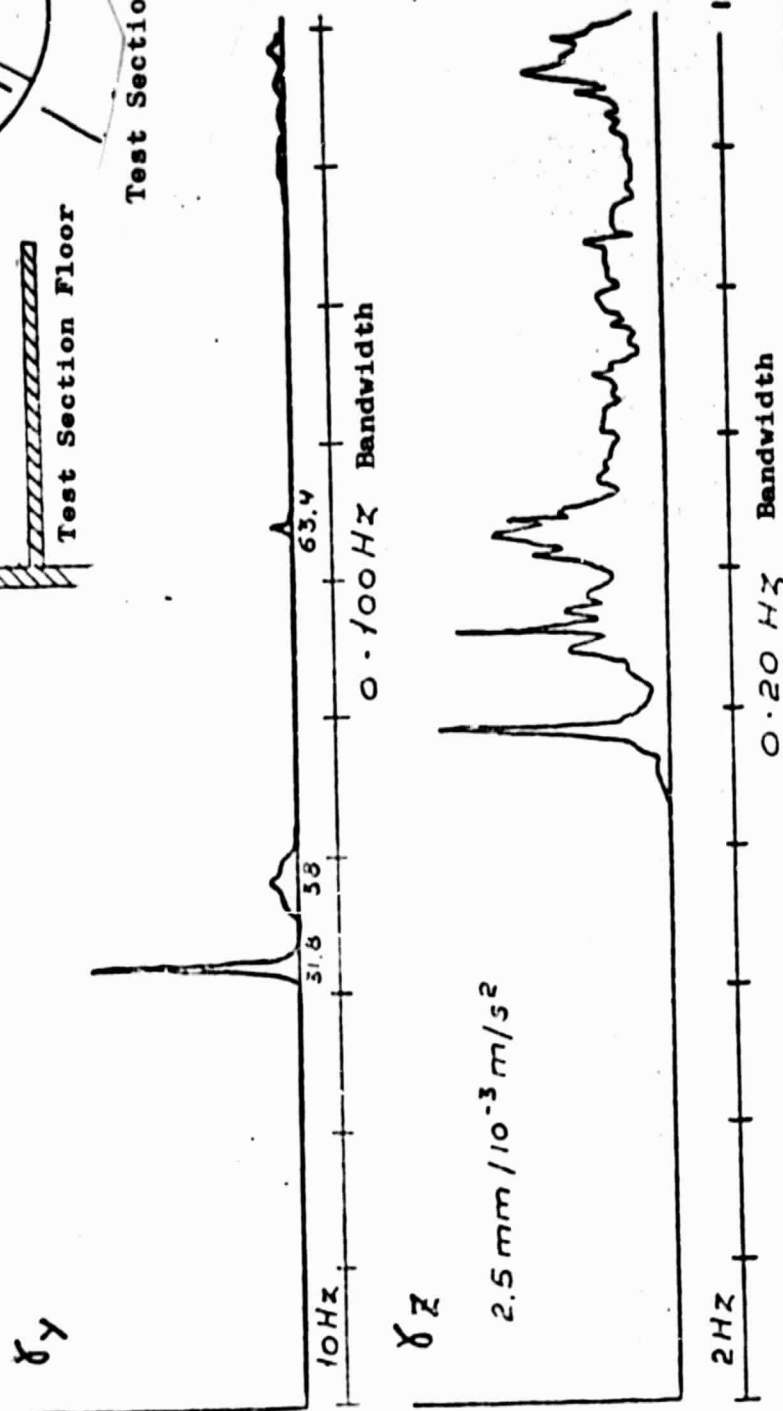
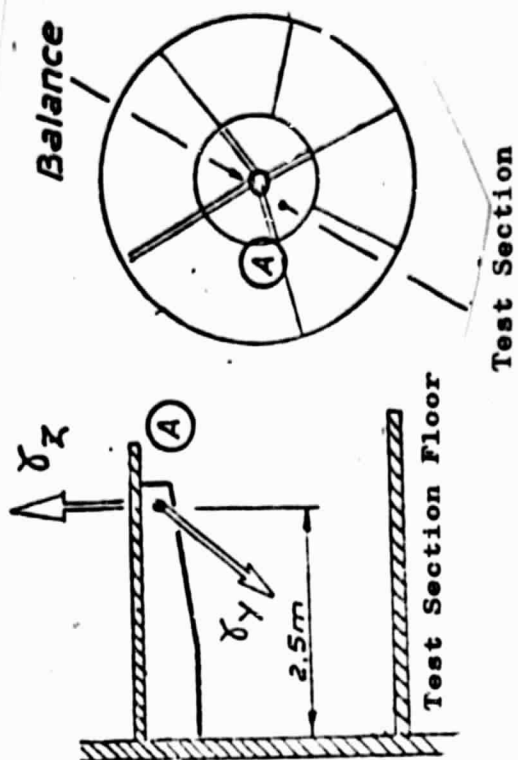
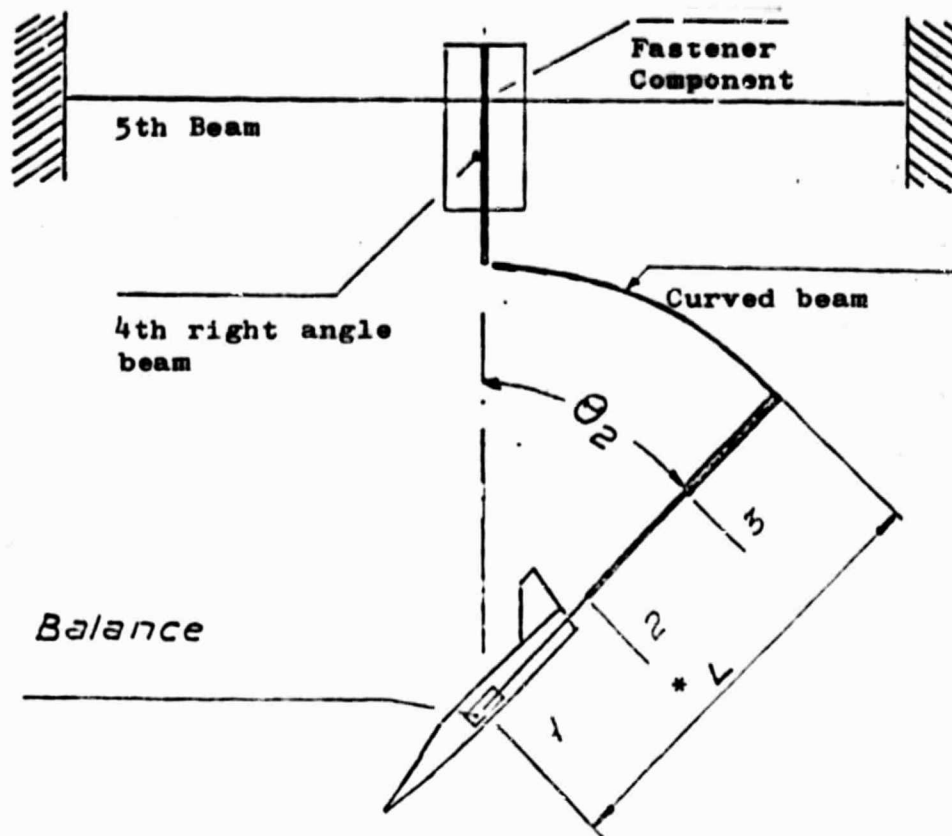


Figure 6



*Right angle beams

MODELLING OF THE ASSEMBLY STRUCTURE

Computational Case

$$\theta_2 = 0^\circ, 45^\circ \text{ AND } 90^\circ$$

2 types of balance: 5 or 6 components.

Model: 50 Kg.

Sting length.

Sting sections and curved sector

Figure 7

ORIGINAL PAGE IS
OF POOR QUALITY

STRUCTURAL MODES OF THE ROTARY ASSEMBLY

.EXCITATIONS BY SHOCKS

.MEASUREMENT ON 5 COMPONENT BALANCE

TEST CASE: 32 Kg MODEL

.COUPLINGS WITH PULSATIONS

$$\lambda . \varphi . \psi = 0$$

$$\theta_2 = 45^\circ$$

$$\theta \leftrightarrow Z \quad \text{AND} \quad \psi \leftrightarrow Y$$

EXCITATION ON

M O D E S	ROLL	φ	21 Hz	/	} contribution balance
	PITCHING	θ	16 Hz	/	
	YAWING	ψ	14 Hz	/	
	Y		10 Hz	10 Hz	} contribution ASSEMBLY
	Z		12 Hz	12 Hz	

Figure 9

STRUCTURAL EXCITATIONS DUE TO V OR U

ANALYSIS OF SIGNALS FROM THE BALANCE

23 Kg Model

Test Case	CONDITIONS	RATE	Ω	noises
1	Δ φ, θ, λ	0	0	none
2	Δ φ, θ, λ	0	123 °/s	very low level
3	$\theta_2 = 0$ $\varphi = 0$ $\lambda = 5$	40 m/s	0	very low level structural modes
4	$\theta_2 = 0$ $\varphi = 0$ $\lambda = 30$	40 m/s	0	very high level structural modes
5	$\theta_2 = 9$ $\varphi = 0$ $\lambda = 0$	40 m/s	123 °/s	very low level structural modes

Figure 10

AERODYNAMIC NOISE S.V.4

STATIC Δp

IN THE TEST CHAMBER

MEASUREMENTS TAKEN IN THE PRESENCE OF THE ASSEMBLY

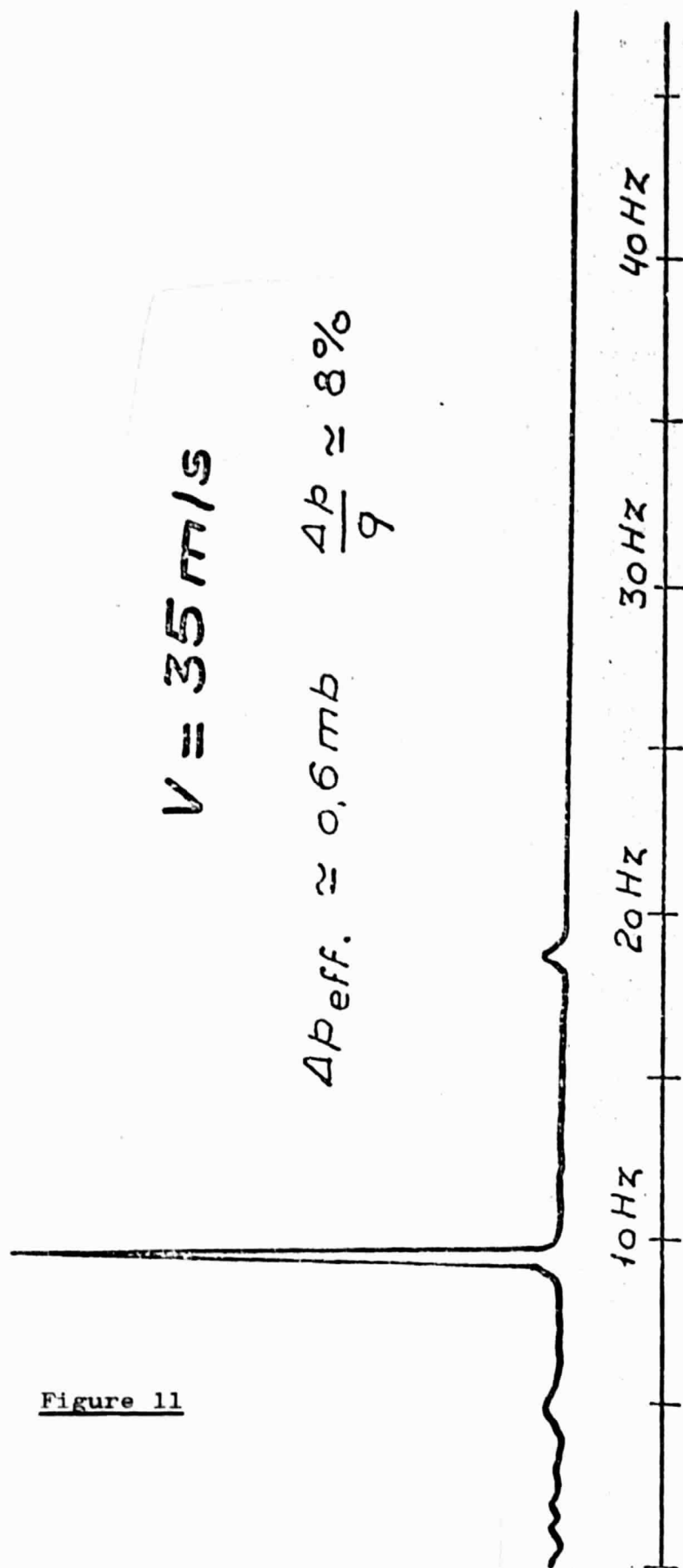


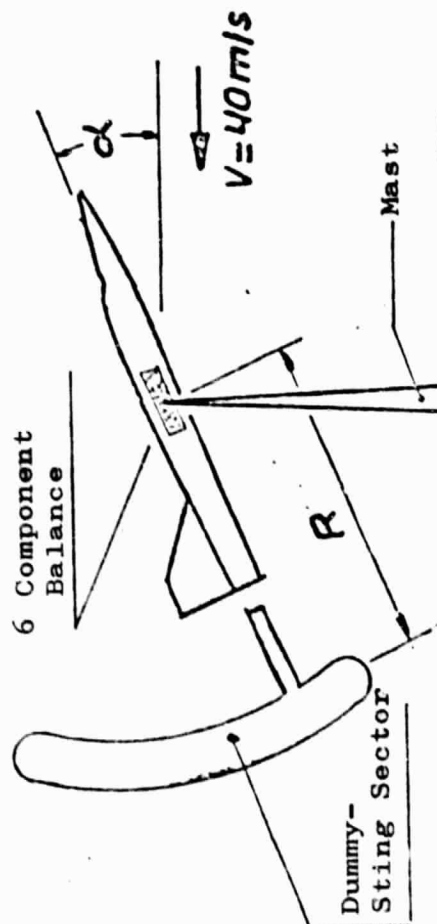
Figure 11

ASSEMBLY - MODEL
AERODYNAMIC INTERFERENCES

ORIGINAL PAGE IS
OF POOR QUALITY

S.V.4 LILLE TESTS
CUSTOM DESIGNED MODEL AND MOUNTING

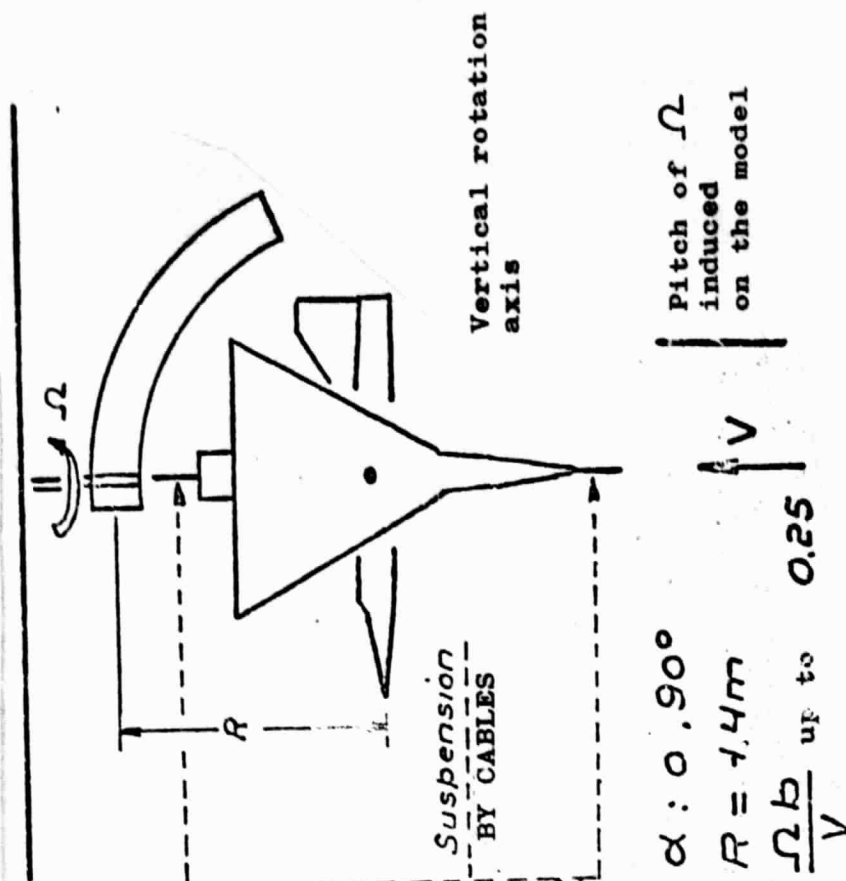
TESTS 55.70
MODEL 42000 1/8.6



FOR $0 < \alpha < 45^\circ$

$R = 1.4m$ (optimum)

No interactions can be detected on C_x , C_z .
Efficiency of control surfaces maintained
Stability increased to a max. of 5%/o



$\alpha : 0.90^\circ$

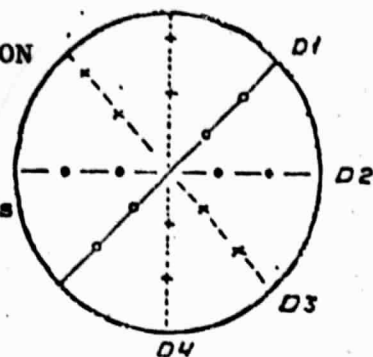
$R = 1.4m$

$\frac{\Omega b}{V}$ up to 0.25

Figure 12

EXPLORATION OF THE TEST SECTION
ORIGINAL CONFIGURATION
WITHOUT BALANCE

Test speeds: 20 m/s and 40 m/s



Inlet of neck-piece

Inlet of the test section

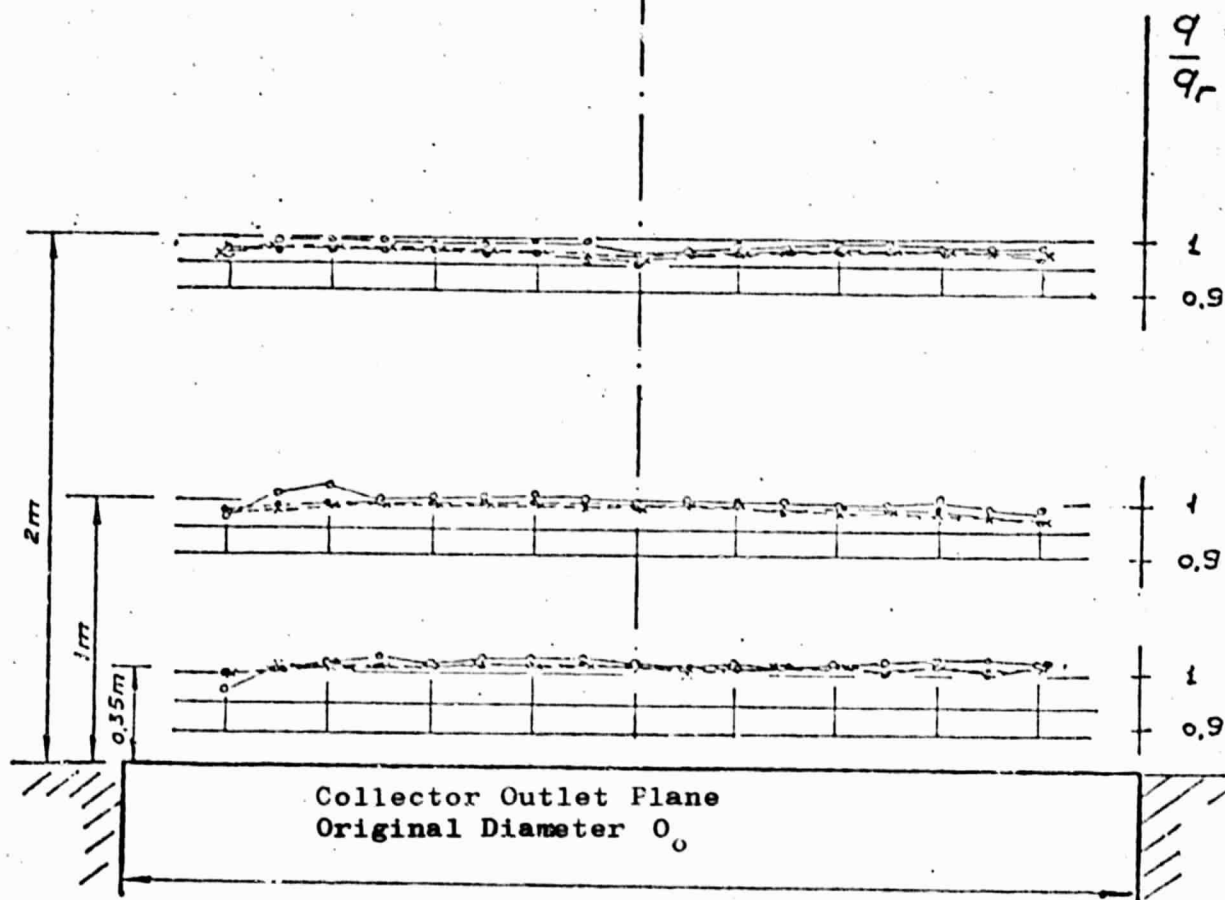


Figure 13

EXPLORATION OF THE TEST SECTION
ORIGINAL CONFIGURATION
WITH BALANCE

Test speed: 20 m/s

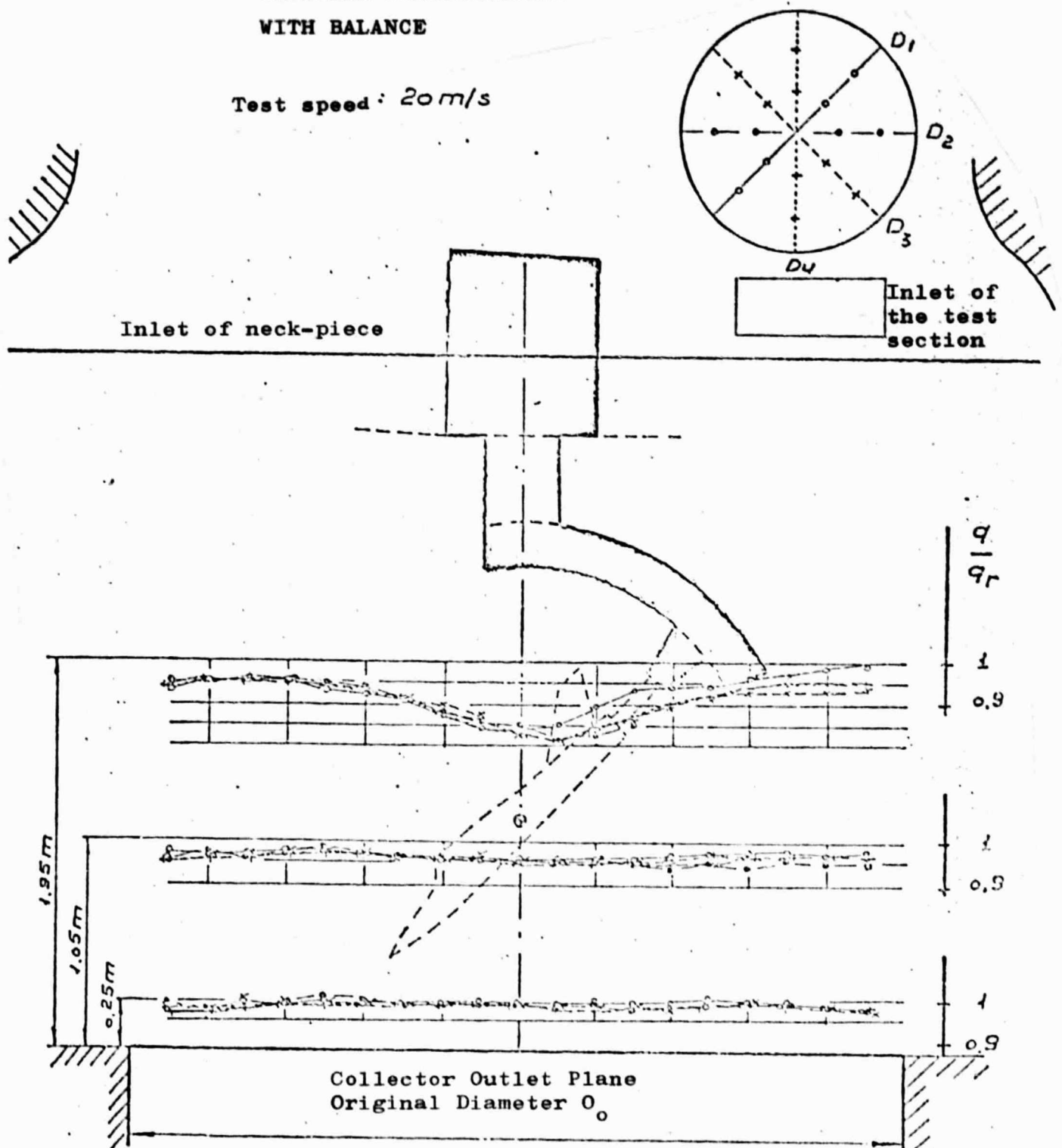


Figure 14

COLLECTOR OUTLET SECTION ON THE AXIAL SPEED GRADIENT

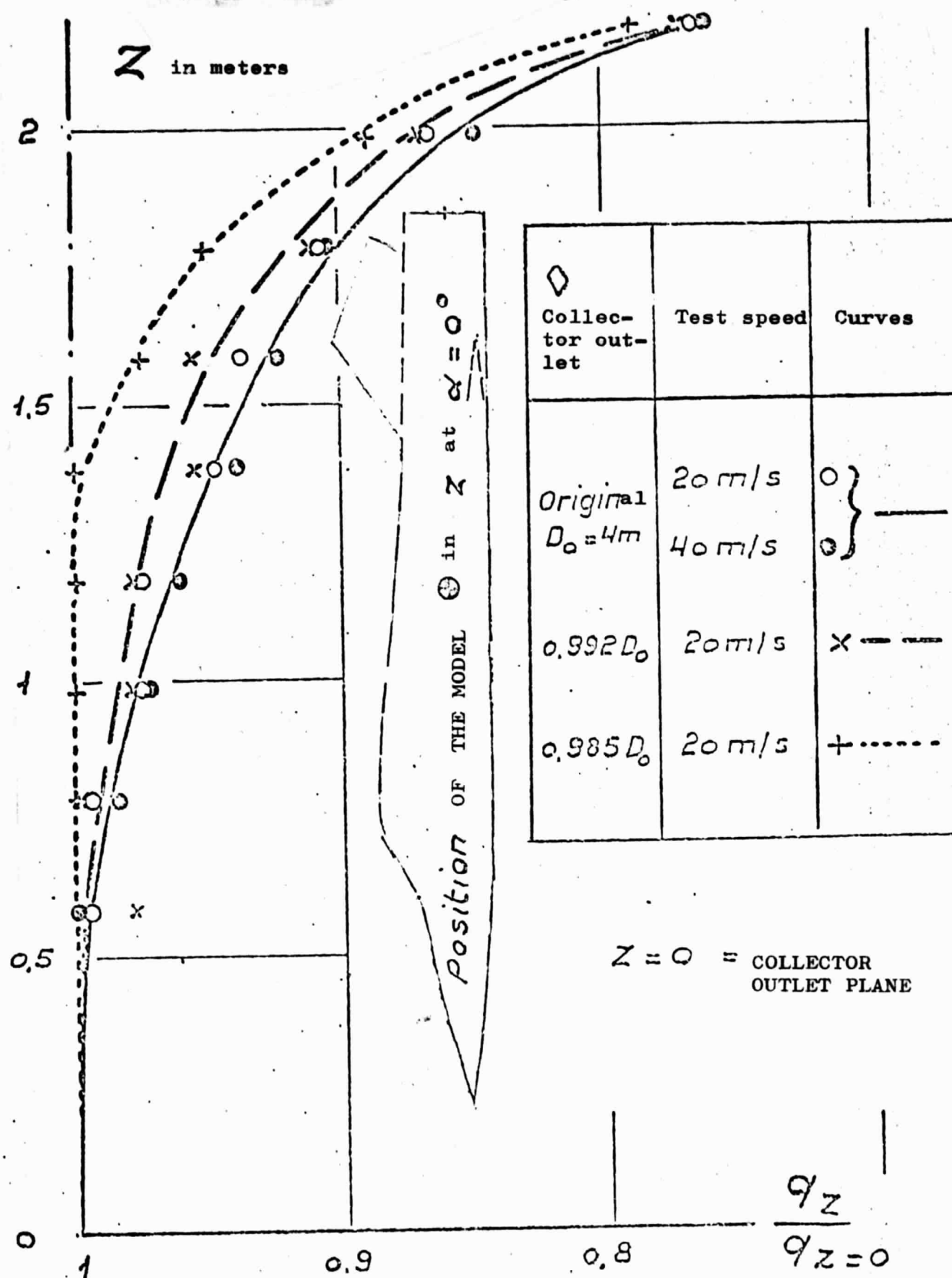


Figure 15

EXPLORATIONS OF THE TEST RANGE
ANEMOCLINOMETRY

RESULTS

• $V: \lambda, \theta_2, \psi, \bar{m} = .95718 = \frac{q_{ce}}{q_{collector}}$

• $\frac{\bar{p}_{stat}}{z} = .3 \text{ m bar/m}$
 $\frac{\partial}{\partial} V = 40 \text{ m/s}$

• $\Delta \alpha \text{ Local} < 2^\circ$

! Law of risk correction

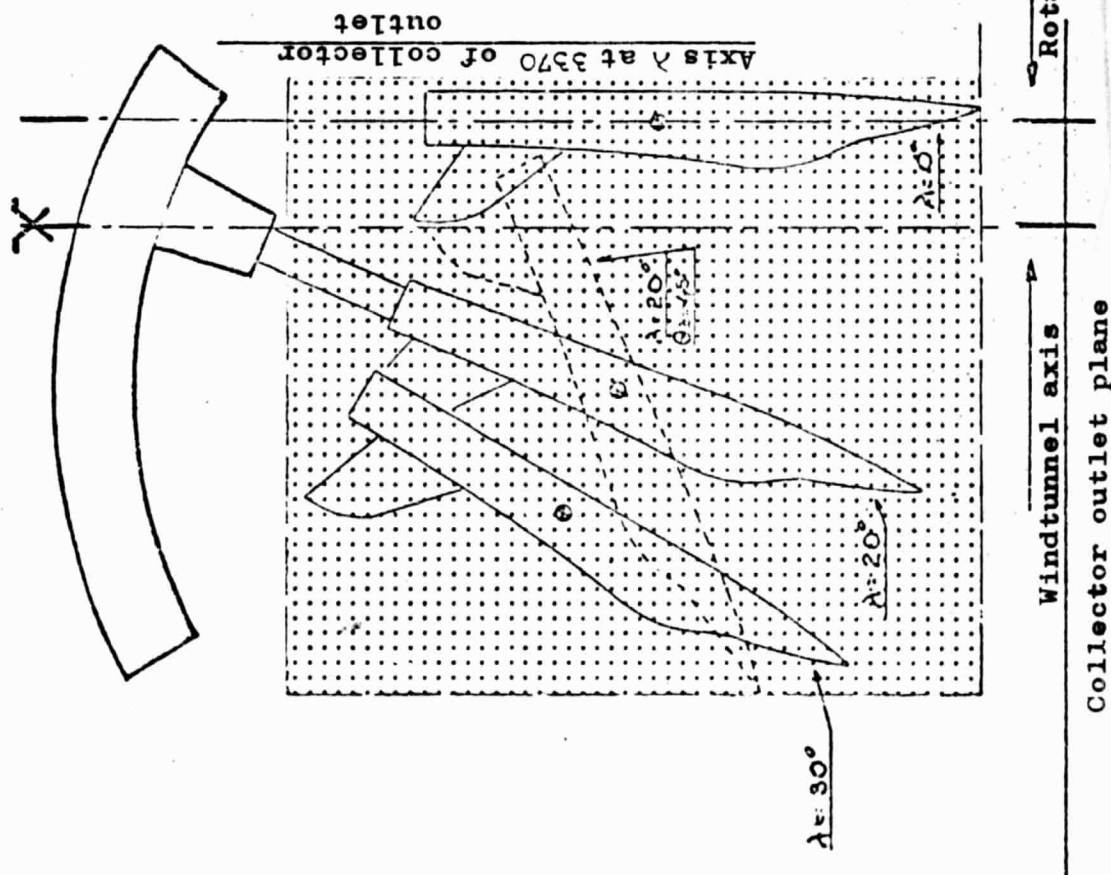


Figure 16

ORIGINAL PAGE IS
OF POOR QUALITY

GENERAL METHOD OF PREPARING
AERODYNAMIC CORRECTIONS

Test case - Measurement of polars

		C. G. Fixed	Influences
1	Scanning $\theta_2, \psi = 0$	yes	θ_2
2	Scanning $\lambda, \psi = 0$	no	$1 \leftrightarrow 2$ λ
3	Scanning $\theta_2, \psi = 180^\circ$	yes	$1 \leftrightarrow 3$ ψ
4	Scanning $\lambda, \varphi = 180^\circ, \psi = 0$	no	$1 \leftrightarrow 4$ $\lambda + \varphi$ $2 \leftrightarrow 4$ φ
5	Scanning $\lambda, \varphi = 0, \psi = 0$ θ_2 set	no	$1, 2 \leftrightarrow 5$ $\lambda + \theta_2$
6	Rotation Ω very weak $\varphi = 0, \theta_2$ set	yes	ψ

Figure 17

SECTION DRIFT

EFFECT OF
HEADING

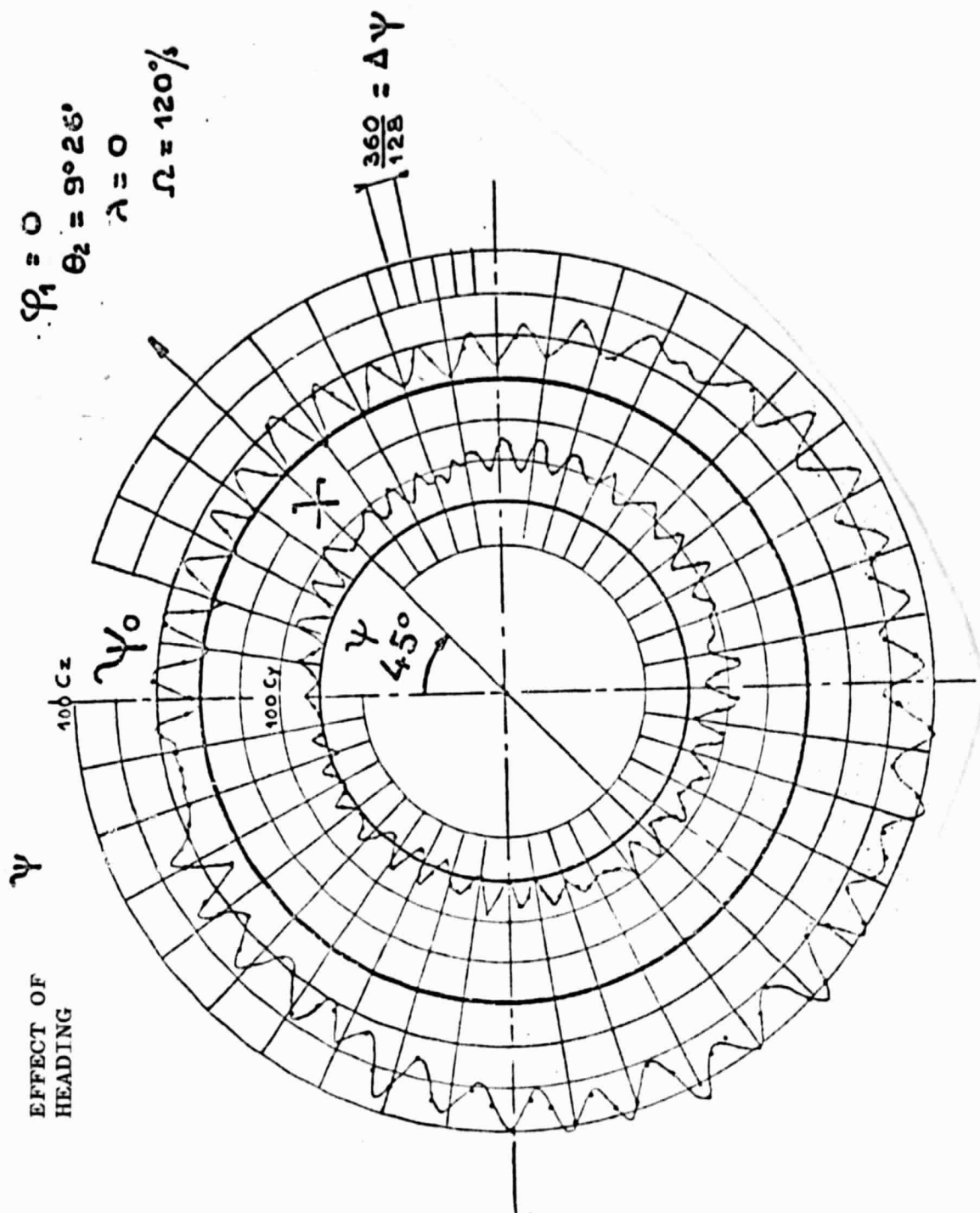


Figure 18

ORIGINAL PAGE IS
OF POOR QUALITY

Key for figure 19:

a-Angular coders; b-Conditioning electronics; c-Conditioners;
d-Gage bridges; e-Filter; f-P.C.M. coder; g-Line transmitter;
h-Actuators; i-Balance visualization; j-Over-all visualization;
k-Remote control decoder; l-Line receptor; m-Ground transducers;
n-Filter conditioning electronics; o-P.C.M. Chain - Frequency of
maximum bits: 130 kB - Sampling frequency per parameter: 700 Hz -
Word length of 12 bits; p-Line transmitter; q-Line receiver;
r-Primary synchronization; s-Secondary synchronization; t-Multi-
channel tape recorder; u-Transposer; v-Remote control coder; w-Multiple
digital interface; w-Simplex exchange unit; x-Printer; y-Plotter;
z-Computer; * Control unit; **Computer bus; *** Illegible.

Key for figure 20:

a-Raw data; b-Checking of signals; c-Saturation control; d-Synchronous
losses; e-Low pass filter without phase shift; f-Control - mean values -
standard deviations; g-Dynamic torque check; h-Test - Average value of
zeros; i-Low-pass; j-Band rejection filter; k-Line rejection filter;
l-Balance matrix - calibrations; m-Over-all aerodynamic coefficients
and parameters.

COMPUTER ROOM

VERTICAL WINDTUNNEL

Control room

In the section

Rotary switches

Transducers

Balance

Test No.

Interface

a

b

c

d

e

f

g

h

i

j

k

l

m

n

o

p

q

r

s

t

u

v

w

x

y

z

AA

BB

CC

DD

EE

FF

GG

HH

II

JJ

KK

LL

MM

NN

OO

PP

QQ

RR

SS

TT

UU

VV

WW

XX

YY

ZZ

AA

BB

CC

DD

EE

FF

GG

HH

II

JJ

KK

LL

MM

NN

OO

PP

QQ

RR

SS

TT

UU

VV

WW

XX

YY

ZZ

AA

BB

CC

DD

EE

FF

GG

HH

II

JJ

KK

LL

MM

NN

OO

PP

QQ

RR

SS

TT

UU

VV

WW

XX

YY

ZZ

AA

BB

CC

DD

EE

FF

GG

HH

II

JJ

KK

LL

MM

NN

OO

PP

QQ

RR

SS

TT

UU

VV

WW

XX

YY

ZZ

AA

BB

CC

DD

EE

FF

GG

HH

II

JJ

KK

LL

MM

NN

OO

PP

QQ

RR

SS

TT

UU

VV

WW

XX

YY

ZZ

AA

BB

CC

DD

EE

FF

GG

HH

II

JJ

KK

LL

MM

NN

OO

PP

QQ

RR

SS

TT

UU

VV

WW

XX

YY

ZZ

AA

BB

CC

DD

EE

FF

GG

HH

II

JJ

KK

LL

MM

NN

OO

PP

QQ

RR

SS

TT

UU

VV

WW

XX

YY

ZZ

AA

BB

CC

DD

EE

FF

GG

HH

II

JJ

KK

LL

MM

NN

OO

PP

QQ

RR

SS

TT

UU

VV

WW

XX

YY

ZZ

AA

BB

CC

DD

EE

FF

GG

HH

II

JJ

KK

LL

MM

NN

OO

PP

QQ

RR

SS

TT

UU

VV

WW

XX

YY

ZZ

AA

BB

CC

DD

EE

FF

GG

HH

II

JJ

KK

LL

MM

NN

OO

PP

QQ

RR

SS

TT

UU

VV

WW

XX

YY

ZZ

AA

BB

CC

DD

EE

FF

GG

HH

II

JJ

KK

LL

MM

NN

OO

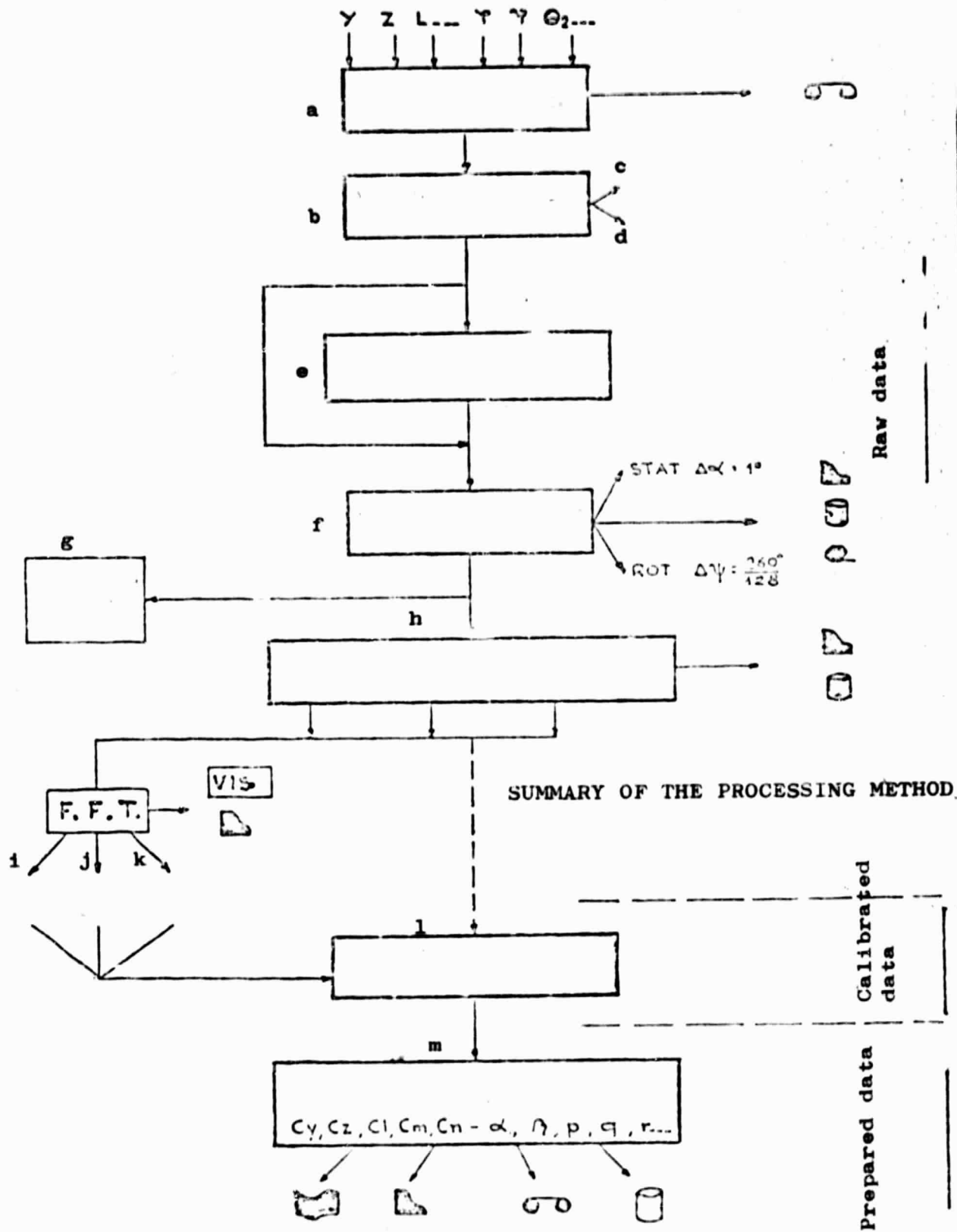


Figure 20

MEASUREMENT - COLLECTION - PROCESSING FREQUENCY CHARACTERISTICS

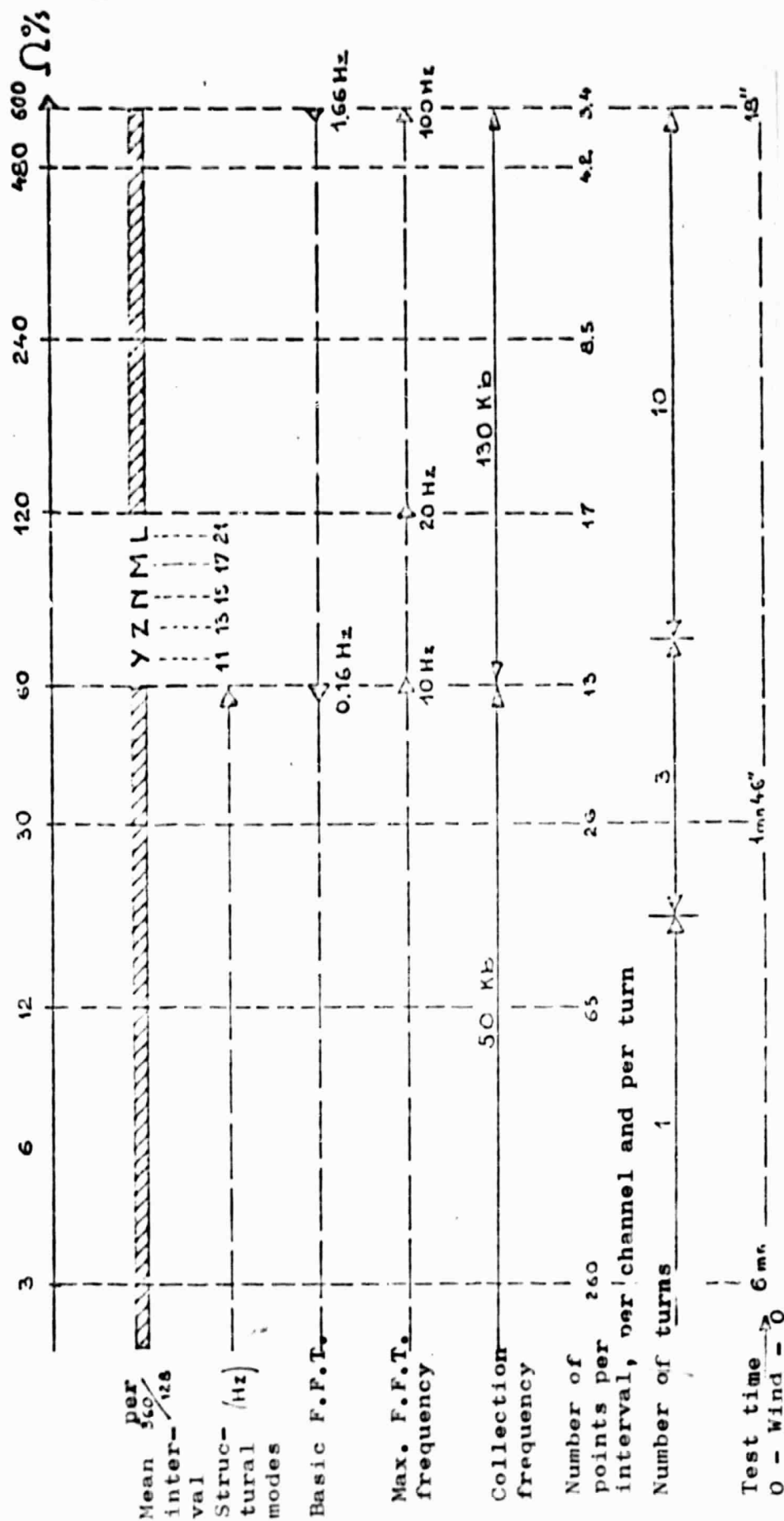


Figure 21

ORIGINAL PAGE IS
OF POOR QUALITY

F.F.T. FILTER OPTIONS

ROTATION TEST
EFFECT OF THE FILTER SYSTEM

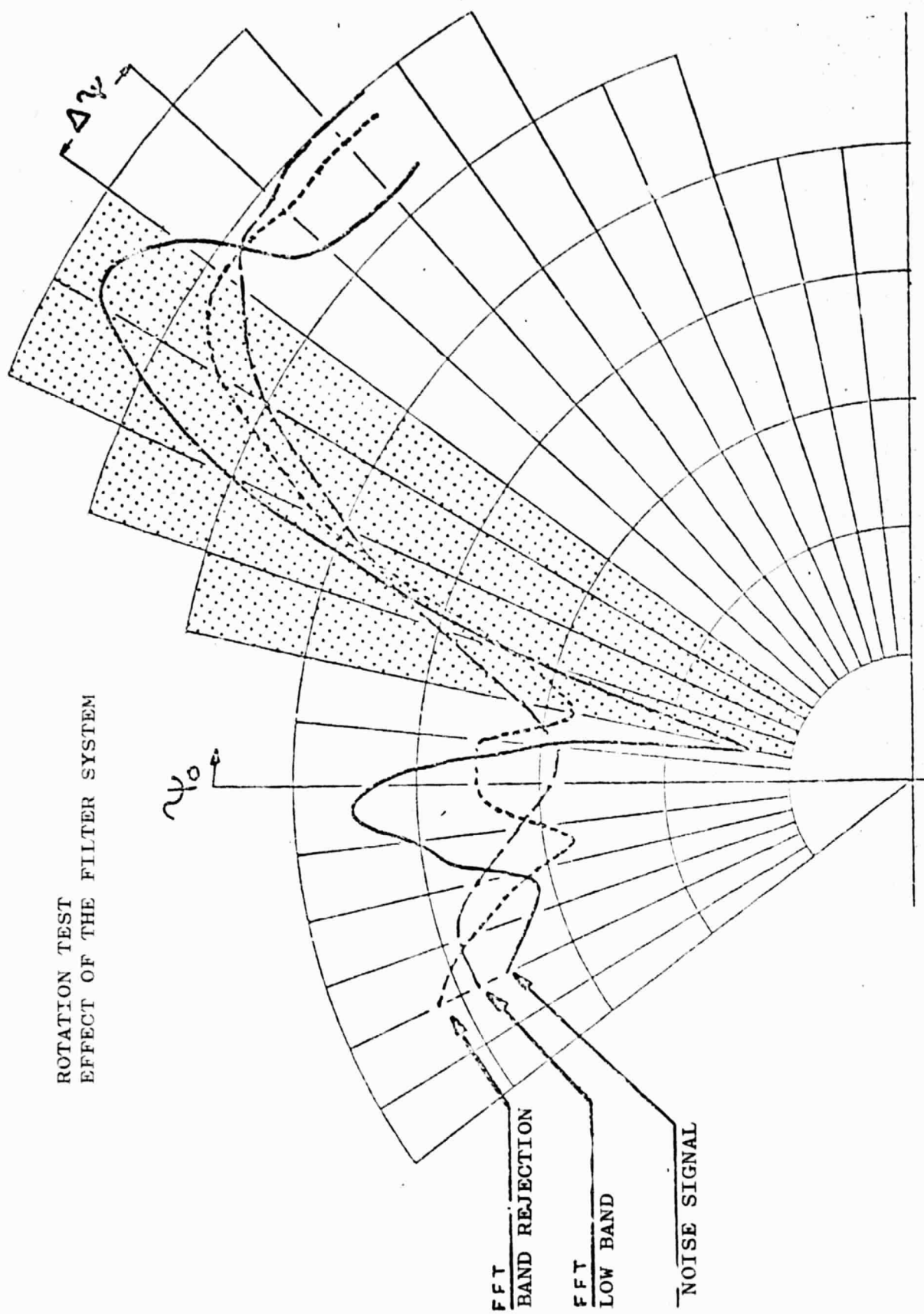


Figure 22